ORIGINAL RESEARCH

A Method for Imaging the Ischemic Penumbra with MRI using IVIM

Mira M. Liu, Niloufar Saadat, Steven P. Roth, Marek A. Niekrasz, Mihai Giurcanu, Mohammed Salman Shazeeb, Timothy J. Carroll, Gregory A. Christoforidis

ABSTRACT

BACKGROUND AND PURPOSE: In acute ischemic stroke, the amount of "local" CBF distal to the occlusion, i.e. all blood flow within a region whether supplied antegrade or delayed and dispersed through the collateral network, may contain valuable information regarding infarct growth rate and treatment response. DSC CBF using a local arterial input function (AIF) is one method of quantifying local CBF (local-qCBF) and correlates with collaterals. Similarly, intravoxel incoherent motion MRI (IVIM) is "local", with excitation and readout in the same plane, and a potential alternative way to measure local-qCBF. The purpose of this work was to compare IVIM local-qCBF against DSC local-qCBF in the ischemic penumbra, compare measurement of perfusion-diffusion mismatch (PWI/DWI), and examine if local-qCBF may improve prediction of final infarct.

MATERIALS AND METHODS: Eight experiments in a pre-clinical canine model of middle cerebral artery occlusion were performed; native collateral circulation was quantified via x-ray DSA 30 minutes post-occlusion, and collateralization was subsequently enhanced in a subset of experiments with simultaneous pressor and vasodilator. IVIM and DSC MRI were acquired 2.5hr post-occlusion. IVIM was post-processed to return local-qCBF from fD*, water transport time (WTT) from D*, diffusion from D, and the PWI/DWI mismatch. These were compared with DSC parameters processed first with a standard global-AIF and then with a local-AIF. These DSC parameters included time-to-maximum, local MTT, standard-qCBF, local-qCBF and PWI/DWI mismatch. Infarct volume was measured with DWI at 2.5hrs and 4hrs post-occlusion.

RESULTS: 2.5hr post-occlusion, IVIM local-qCBF in the non-infarcted ipsilateral territory strongly correlated with DSC local-qCBF (slope=1.00, R^2=0.69, Lin's CCC=0.71). Correlation was weaker between IVIM local-qCBF and DSC standard-qCBF (R^2=0.13). DSC local-qCBF and IVIM local-qCBF in the non-infarcted ipsilateral territory both returned strong prediction of final infarct volume (R^2=0.78, R^2=0.61 respectively). DSC standard-qCBF was a weaker predictor (R^2=0.12). The hypoperfused lesion from DSC local-qCBF and from IVIM local-qCBF both predicted final infarct volume with good sensitivity and correlation (slope=2.08, R^2=0.67, slope=2.50, R^2=0.68 respectively). The IVIM PWI/DWI ratio was correlated with infarct growth (R^2=0.70) and WTT correlated with DSC MTT (R^2=0.60).

CONCLUSIONS: Non-contrast IVIM measurement of local-qCBF and PWI/DWI mismatch may include collateral circulation and improve prediction of infarct growth.

ABBREVIATIONS: AIF: arterial input function, IVIM: intravoxel incoherent motion, qCBF: quantitative cerebral blood flow, WTT: water transport time, MCAO: middle cerebral artery occlusion, MD: mean diffusivity

Received month day, year; accepted after revision month day, year.

From the Department of Radiology, Medical Physics (MML, TJC), Department of Interventional Radiology (NS, GAC), Department of Surgery and Large Animal Studies (MAN), and the Department of Statistics (MG), University of Chicago, Chicago, IL, USA; Department of Anesthesiology (SPR), University of Illinois, Chicago, IL, USA; Department of Radiology (MSS), University of Massachusetts Chan Medical School, Worcester, MA, USA; Department of Radiology, Biomedical Engineering and Imaging Institute (Current affiliation MML), Icahn School of Medicine at Mount Sinai, New York, NY, USA; Mount Carmel Health Systems (Current affiliation GAC), Columbus, OH, USA.

The authors declare no conflicts of interest related to the content of this article.

Please address correspondence to Mira M. Liu, PhD, Department of Radiology, BioMedical Engineering and Imaging Institute, Icahn School of Medicine at Mount Sinai. 1470 Madison Ave, New York, NY 10029, USA; Liusarkarm@uchicago.edu.

SUMMARY SECTION

PREVIOUS LITERATURE: In ischemic stroke, the "local" nature of IVIM with excitation and readout in the same plane allows it to image all capillary motion. This includes blood flow from the collateral network even if it arrives delayed and dispersed compared to antegrade flow. Similarly, correcting DSC quantitative CBF (qCBF) for this delay and dispersion using a local arterial input function has shown improved agreement with collateral score. While IVIM in stroke has predominately been compared to standard DSC, comparison of IVIM local-qCBF to DSC local-qCBF may improve agreement and demonstrate how local-qCBF could add valuable information to stroke imaging.

KEY FINDINGS: In a canine model of middle cerebral artery occlusion, IVIM local-qCBF in the ipsilateral MCA territory correlated strongly with DSC local-qCBF (R^2=0.69), and weakly with DSC standard-qCBF (R^2=0.16). Local-qCBF returned stronger prediction of final infarct volume (DSC R^2=0.78, IVIM R^2=0.61) than standard-qCBF (R^2=0.12). IVIM PWI/DWI ratio was strongly correlated with infarct growth (R^2=0.70).

KNOWLEDGE ADVANCEMENT: These findings support (1) IVIM as a non-contrast method of measuring local-qCBF, including collateral circulation, in acute stroke, (2) improved agreement of IVIM and DSC with a local-AIF, and (3) using simultaneous perfusion-weighted and diffusion-weighted images from IVIM for PWI/DWI mismatch.

INTRODUCTION

Acute ischemic stroke occurs when sudden loss of blood supply to a region of the brain leads to damaged or dead brain cells. Rapid early intervention by thrombectomy or thrombolysis after symptom onset[1] is most effective in treating stroke[2,3]. However, large multi-center trials[4-6] have suggested that the treatment window can be extended for some patients. This "late thrombectomy" can be performed 6 to 24 hours after symptom onset, which is a crucial extension for patients with unknown onset time. MRI can be used to assess if a patient may undergo late thrombectomy based on a "mismatch" between (1) the hypoperfused lesion distal to an occlusion imaged with PWI and (2) the amount of irretrievable, dead/infarcted brain imaged with DWI[7,8] . This "PWI-DWI mismatch" is one way to measure the ischemic penumbra[9,10]. Accurate measurement of this mismatch may be useful for patient triage if the time of onset is unknown, and for imaging the penumbra in novel stroke therapeutic studies[11-13].

Hypoperfusion can be measured as prolonged time-to-maximum (Tmax) or delayed arrival time of the contrast bolus[14]. However, even when delayed bolus makes regions of the brain *appear* hypoperfused, some of these regions may be sustained by collateral circulation[15,16]. "Local" CBF distal to the occlusion, i.e. all blood flow whether supplied antegrade or delayed and dispersed through the collateral network, is one way of measuring this collateral circulation. Including collateral circulation in perfusion imaging may provide more complete pathophysiologic information for each patient, improve patient selection for reperfusion therapy, and better predict infarct growth[15-17]. Recently, DSC CBF with a local-arterial input function (AIF) has been shown to measure local quantitative CBF (local-qCBF in ml/100g/min) that correlates with collateralization and infarct growth better than standard DSC[18]. Similarly, intravoxel incoherent motion MRI (IVIM) perfusion fraction has shown promise as a method of imaging collateral flow[19]. As such, imaging local-qCBF with IVIM may add valuable information about collateral circulation, hypoperfusion in the ischemic penumbra, and infarct growth.

This work examines the use of non-contrast IVIM to measure local-qCBF and measure the ischemic penumbra in acute ischemic stroke. To study the nature of the local flow, IVIM parameters are compared to both local-AIF DSC and standard DSC parameters in a pre-clinical canine model of acute middle cerebral artery occlusion (MCAO). First, it compares IVIM local-qCBF to DSC local-qCBF and to DSC standard-qCBF in the ischemic penumbra. Second, it compares the predictive ability of hypoperfusion lesions from local-qCBF versus standard-qCBF against final infarct. Finally, it uses IVIM simultaneous local-qCBF PWI and DWI ratio to predict infarct growth and compares it to the PWI/DWI ratio from DSC Tmax, DSC local-qCBF, and DSC standard-qCBF.

MATERIALS AND METHODS

Theory

Contrast bolus is delayed and dispersed when traveling around an occlusion through the collateral network. Mathematically, standard DSC perfusion analysis may not include compensatory blood that travels through collaterals if this delay is not corrected for. This means that standard DSC without correction may overestimate the hypoperfusion lesion if there are good collaterals. Use of a voxel-wise local-AIF has been shown to correct for this delay[18,20,21]. With a local-AIF generated for every voxel, rather than a standard single global-AIF in a brain-feeding artery, DSC local-qCBF was shown to capture the perfusion in a voxel *including* collateral circulation[18].

In theory, IVIM local-qCBF in the penumbra should agree more closely with DSC local-qCBF than standard DSC, especially in cases with good collateral circulation. This is because IVIM is local with excitation and readout in the same plane[24]. It measures capillary flow independent of contrast bolus arrival by separating motion into blood pseudo-diffusion and tissue diffusion[22]. Both Local-AIF DSC and IVIM should be sensitive to all the blood in capillaries, whether supplied antegrade or retrograde through the collateral network[18,19]. The speed of the capillary motion can also estimate how long it would take for 50% of the original molecules in a volume to diffuse out[23]; this theoretically could be comparable to local-AIF DSC mean transit time. Further detail of the theory behind local-qCBF is available in the online supplemental.

Pre-clinical Canine Model

All experiments were conducted using a previously reported preclinical canine model of ischemic stroke[24]. The two-day experimental protocol was approved by the University of Chicago Institutional Animal Care and Use Committee and reported in compliance with ARRIVE guidelines. The University of Chicago is an AAALAC International accredited institution adhering to the following guidelines, regulations, and policies: a) Guide for the Care and Use of Laboratory Animals (National Research Council), b) USDA Animal Welfare Act and Animal Welfare Regulations, and c) Public Health Service Policy on Humane Care and Use of Laboratory Animals.

Eight canines (mean age = 3.4±3.9y, mean weight = 25.3±5.0kg, 7 female, 1 male) underwent permanent endovascular MCAO via embolic occlusion coils under fluoroscopic guidance with R/L randomization. M1 occlusion was verified via selective internal carotid and vertebral arteriography[24]. Native collateral circulation was quantified 30 minutes post-MCAO by assessing X-ray arteriographic images (OEC9800; General Electric Healthcare, Chicago, IL) with a pial collateral score[25] modified for canines as described previously[16]. Further detail of the canine model and collateral scoring is available in the online supplemental. To evaluate a larger range of collateral supply, five of eight subjects underwent flow augmentation (simultaneous pressor and vasodilator norepinephrine and hydralazine); treated and untreated subjects were pooled. In previous work, this flow augmentation has been shown to increase collateral circulation and slow infarct growth by disruption of cerebral autoregulation of poor collaterals[13,26].

MRI Acquisition

MRI was acquired 2.5 hours after occlusion with a 3T MRI scanner (Ingenia, Philips) head-first, prone position with a 15 channel receive-only coil. Sequences were acquired with DSC followed by DTI and then IVIM.

DSC images (coronal plane, 2D gradient echo, T2*-weighted EPI, FOV/Matrix=160mm/176, 5 slices/6mm thick, TR/TE=500/30, 120

phases, total scan time = 60s) were taken along with rapid 15s T1 maps following the "T1-bookend method"[20,21,27-33] (2D Inversion Recovery (IR) Look Locker, single-shot EPI FOV/Matrix=160mm/176, 5 slices/6mm thick). Gadolinium (Gd)-based contrast agent (Multihance, Bracco, Princeton, NJ, USA) followed by a saline flush (Gd: 3mL at 2mL/s, saline: 20mL at 2mL/s) was injected in forepaw.

DTI for mean diffusivity (MD), analogous to more widely used ADC, was acquired to measure infarct volume every 30 minutes post-MCAO and track infarct growth over time[16]. A stack of 50 2D DTI slices was prescribed to cover the entire head (slice thickness= 2mm, FOV =128x128 mm/matrix = 128x128, TR/TE = 2993/83ms, FA = 90°, b-values = 0, 800 s/mm^2, 32 directions).

Multi b-value DWI for IVIM were collected with 10 b-values (0,111, 222, 333, 444, 556, 667, 778, 889, 1000s/mm2) and 3 orthogonal directions. Scans covered the entire head (2D single shot EPI, TR/TE= 3056/91ms, 50 slices/2mm thick, FOV/Matrix = 224mm/128 or FOV/Matrix 160mm/96, total scan time = 5.5 mins, SENSE Factor=2). MR protocol is available in the online supplemental.

DSC Analysis

DSC local-qCBF was post-processed in ml/100g/min using the well-established T1-bookend method[20,21,27-33] with a voxel-by-voxel local-AIF. This local-AIF corrected for the late arrival (delay) and "blunting" (dispersion) of the contrast bolus as it propagated through the brain[21] and included collateral supply in the ischemic penumbra[18].

DSC was also processed with a standard single global-AIF and quantified as standard-qCBF with the same T1-bookend method. Tmax was calculated as the time at which the residue function reached its maximum after deconvolution from the global-AIF. Further detail of the T1-bookend method and processing with the two AIFs is available in the online supplemental.

DWI Analysis

DWI core infarct was defined, as previously reported[26], as MD<0.00057 mm^2/s from DTI mean diffusivity and converted to binary infarction maps. Final infarct volume was calculated from the DTI taken 4hrs post-MCAO as infarct growth has likely steadied by that time[16,24].

IVIM Analysis

IVIM local-qCBF (in ml/100g/min) and diffusion (in mm^2/s) values were calculated from the 10 b-values using a two-step segmented fit[22,34-38]. IVIM D (tissue-diffusion) was fit on a voxel-wise basis to the second component of the standard IVIM bi-exponential $\frac{S_b}{S_0} = fe^{-bD^*} + (1-f)e^{-bD}$ for b-values>250 s/mm^2. After fitting IVIM D, the pseudo-diffusion components f and D^* were fit to the whole equation using nonlinear least squares. The parameter fD^* was quantified as local-qCBF (in ml/100g/min) using the water transport time (WTT) model[23]: local-qCBF $\approx fD^* \times 93000$ [ml/100g/min]. IVIM core infarct was defined as IVIM D<0.000515 mm^2/s. This threshold was chosen to agree most closely with DWI total core infarct volume using leave-one-out cross-validation from previous study[39]. Further detail on the IVIM post-processing is available in the online supplemental.

After post-processing, the IVIM parameter maps were co-registered and resized to anatomically overlap with DSC images for direct region-of-interest comparison. Three consecutive IVIM slices were averaged to match the coarser DSC slice thickness of 6 mm. Previously reported leave-one-out cross validation *T2* map thresholds[23,39], D^* >0.10 mm^2/s and f >0.30 [19,40] were applied to remove cerebrospinal fluid (CSF) dominated voxels and minimize partial volume effects without use of a *T2*-prepared IR pulse for CSF suppression[36].

qCBF in Ipsilateral MCA Territory and Final Infarct

2.5hrs post-occlusion, the ipsilateral MCA territory was defined as region of the brain that would normally be supplied by the occluded (right or left) MCA. The average values of IVIM local-qCBF and DSC local-qCBF in the ipsilateral MCA territory that was not infarcted (i.e. MD>0.00057 mm^2/s) were compared to each other via linear regression and Bland-Altman. The average DSC and IVIM local-qCBF in this non-infarcted MCA territory were also used to predict final infarct volume by linear regression. IVIM local-qCBF was also compared to DSC standard-qCBF. All analyses were performed in three consecutive 6 mm coronal slices starting at, and posterior to, the M1 segment for both DSC and IVIM images.

qCBF in the Contralateral MCA Territory

The contralateral MCA territory was defined as the region of the brain that was supplied by the not occluded (right or left) MCA. The average values of IVIM local-qCBF and DSC local-qCBF in this contralateral MCA territory were compared to each other via linear regression. IVIM local-qCBF was also compared to DSC standard-qCBF. These analyses were performed in the same three slices as the ipsilateral MCA territory.

2.5hr Hypoperfused Lesion and Final Infarct Volume

The 2.5hr hypoperfused lesion was calculated first as the volume of brain with DSC local-qCBF<26ml/100g/min, second as DSC Tmax>1s[18], and third as IVIM local-qCBF<26ml/100g/min. Correlation of the hypoperfusion lesion against the final 4 hr infarct volume was measured by linear regression. Note that the hypoperfused lesion was independent of DWI measurements; it was only based on thresholded local-qCBF, which could possibly include tissue that had already died. Hypoperfused lesion from standard-qCBF was also calculated by thresholding at 26ml/100g/min.

Perfusion-Diffusion Mismatch Ratio and Infarct Growth

The PWI/DWI volume ratio was calculated from DSC local-qCBF, IVIM local-qCBF, and Tmax values. The PWI volume was defined as the hypoperfused lesion described above. For DSC local-qCBF, standard-qCBF, and Tmax, the DWI volume was the core infarct (MD<0.00057 mm^2/s) volume. For IVIM, the DWI volume was IVIM D<0.000515 mm^2/s. Using IVIM D meant that the IVIM PWI/DWI could use images only from the IVIM sequence and allowed simultaneous PWI and DWI. The PWI/DWI ratio of the hypoperfused lesion

volume to the core infarct volume was compared via linear regression to the change in infarct volume between the time of the perfusion scans and the final 4hr infarct. The PWI/DWI mismatch was also calculated using the standard-qCBF hypoperfused lesion.

Hypoperfusion from Local Temporal Parameters

Hypoperfusion lesions calculated from slowed transit time from local-AIF DSC MTT and IVIM WTT were generated based on varying transit time thresholds from 1-10 s. The volumes from the thresholds were compared to examine correlation and agreement. To reduce the sensitivity to noise, values over 20s were excluded as being "unphysical." More detail on the DSC MTT and IVIM WTT is available in the online supplemental.

Statistics

Linear regression, Bland-Altman, and Lin's Concordance Correlation Coefficient (Lin's CCC) were used to compare IVIM local-qCBF against DSC local-qCBF and standard-qCBF in the MCA territory. Linear regression was used for correlation of local-qCBF and standard-qCBF hypoperfused lesions against DWI final infarct, and for correlation of the 2.5hr PWI/DWI ratio against infarct growth. Paired Wilcoxon signed-rank and linear regression were used to compare all equivalent measures between IVIM, Local-AIF DSC, and standard DSC. All statistical analysis was performed in Python 3.11.4 (Anaconda Inc., 2024). A p-value of <0.05 was considered statistically significant.

RESULTS

83% of the parent study experiments were successful and performed to completion (this current study analyzed the successful cases with completed IVIM, T1-bookend DSC, 2.5hr and 4hr DTI). Access to all results, raw images and tabulated data is available upon request to the corresponding author.

Perfusion and Diffusion Maps

Example images of DSC local-qCBF, IVIM local-qCBF maps, IVIM D, and MD infarct maps acquired 2.5 hrs post-MCAO are shown in Fig.1, with three IVIM slices averaged and resized to match DSC. Subject A was in the control group and had a good native collateral score shown by x-ray angiography. The bottom row shows the corresponding images for Subject B in the control group with a poor native collateral score. Note the pronounced difference in ipsilateral perfusion in a setting of good collaterals (Fig.1A vs Fig.1B). In both cases, IVIM local-qCBF shows similarity with DSC local-qCBF. The corresponding maps of the IVIM D and DTI MD are also shown (Fig.1C-D). Note that in Subject A the perfusion is reduced (Fig.1A), but tissue viability maintained (Fig.1C), whereas in Subject B both DSC and IVIM local-qCBF showed compromised qCBF (Fig.1B) and a large core infarct (Fig.1D) with minimal salvageable PWI-DWI mismatch.

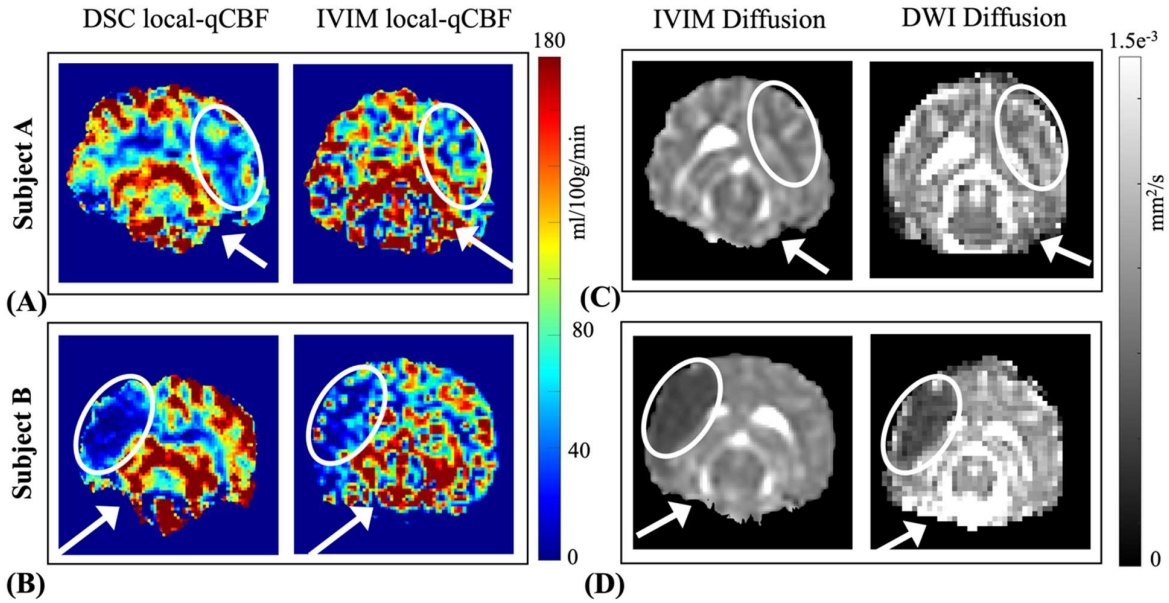

FIG 1. A comparison of local-qCBF in ml/100g/min between DSC and IVIM for subject A with good collateral circulation (A) and subject B with poor collateral circulation (B). DSC was fully quantitative and corrected for arterial delay and dispersion effects, IVIM was quantified with water transport time. The corresponding diffusion maps are shown in (C) and (D), respectively. White arrows denote the position of the MCA coil, white ovals denote the MCA territory. IVIM local-qCBF is averaged across three slices to match the 6mm slice thickness of DSC, and along with an automatic T2 threshold, voxels with $D^*>0.10$ and/or $f > 0.30$ are excluded to remove fast-flowing CSF-dominated voxels.

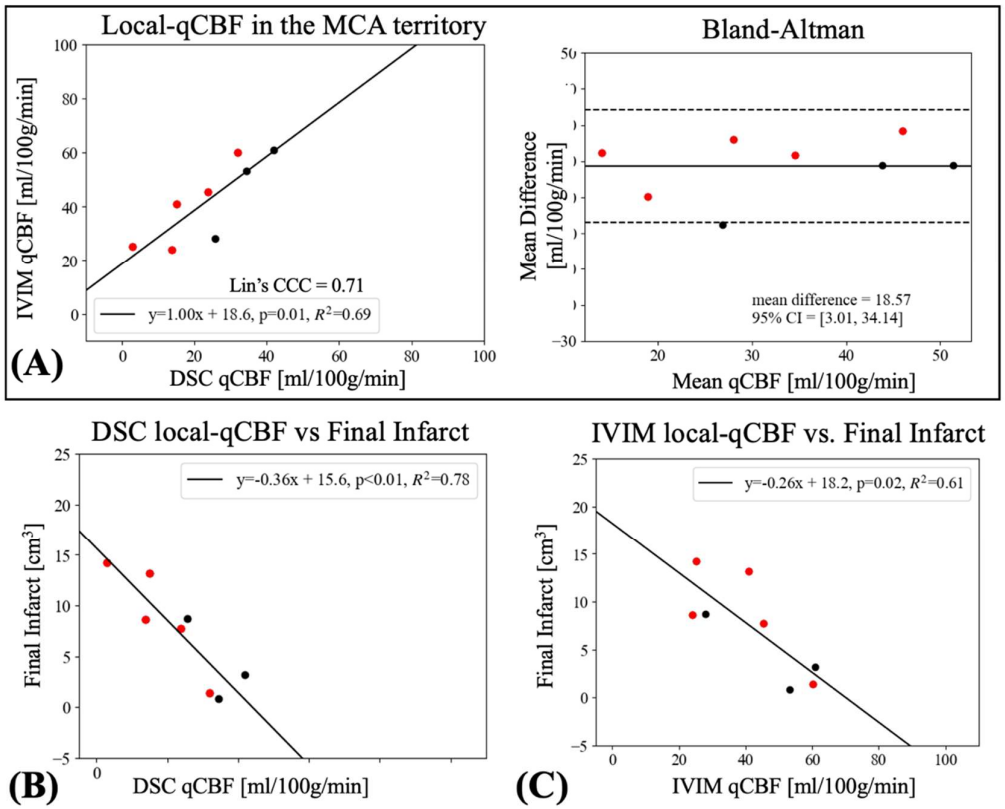

FIG 2. (A) Correlation and linear regression of IVIM local-qCBF against DSC local-qCBF in the non-infarcted MCA territory 2.5 hours post MCAO with corresponding Bland-Altman plot. Final (4 hour) infarct volume correlated against (B) DSC local-qCBF and (C) IVIM local-qCBF. Experiments were pooled over treatment and baseline collateralization to expand the range of collateral circulation. Red represents those that received flow augmentation.

qCBF in the Ipsilateral MCA Territory

DSC and IVIM local-qCBF in the non-infarcted MCA territory strongly correlated (Fig.2A) across collateral status and flow augmentation. Bland Altman showed a significant unbiased mean difference (+19ml/100g/min), with IVIM local-qCBF higher than DSC local-qCBF (Fig.2A, Table 1). In comparison, correlation between IVIM local-qCBF and DSC standard-qCBF was not significant (R^2=0.13, p=0.38). Lower DSC local-qCBF and IVIM local-qCBF in the non-infarcted ipsilateral MCA territory correlated with larger final infarct (Fig.2B-C). DSC local-qCBF was the strongest predictor, and IVIM local-qCBF was also a stronger predictor than DSC standard-qCBF for prediction of final infarct ($p = 0.40$, $R^2 = 0.12$).

Table 1. Comparable parameters between IVIM, Local-AIF DSC, and standard DSC. qCBF is presented in ml/100g/min.

	Local-AIF DSC $\mu \pm \sigma$ (range)	IVIM $\mu \pm \sigma$ (range)	Standard DSC $\mu \pm \sigma$ (range)	IVIM vs. Local-AIF DSC - Wilcoxon signed-rank - Linear Regression	IVIM vs. Standard DSC - Wilcoxon signed-rank - Linear Regresssion
Non-infarcted ipsilateral MCA territory qCBF	23.9±11.6 (4.5-44.7)	38.5±13.5 (34.1-60.8)	17.1±4.9 (6.8-24.7)	t-stat=0.0, p=0.007 R^2=0.73, p=0.01	t-stat= 0.0, p=0.007 R^2=0.13, p=0.38
Contralateral MCA territory qCBF	25.1±14.2 (11.4-47.2)	34.8±11.9 (14.4-57.1)	14.9±5.6 (6.2-25.1))	t-stat = 5.0, p=0.04 R^2=0.57, p=0.02	t-stat= 0.0, p=0.003 R^2=0.46, p=0.05
Hypoperfused lesion volume	2.1±1.1 (0.59-4.2)	2.4±0.7 (1.5-3.9)	3.4±1.3 (1.0-5.8)	t-stat = 12.0, p=0.46 R^2=0.53, p=0.18	t-stat = 8.0, p=0.19 R^2=0.32, p=0.44
PWI/DWI ratio	5.9±6.12 (1.14-18.5)	7.5±7.4 (1.5-19.3)	12.6±16.0 (1.3-41.3)	t-stat = 9.0, p=0.25 R^2=0.74, p=0.005	t-stat = 12.0, p=0.46 R^2=0.81, p=0.002

*AIF: Arterial Input Function, qCBF: quantitative cerebral blood flow, IVIM: intravoxel incoherent motion.

qCBF in the Contralateral MCA Territory

IVIM local-qCBF in the contralateral MCA territory correlated similarly against both DSC local-qCBF and DSC standard-qCBF ($R^2 = 0.57, p = 0.02; R^2 = 0.46, p = 0.05$ respectively). Again, the IVIM returned higher local-qCBF than both versions of DSC (Table 1).

Hypoperfused Lesion Against Final Infarct Volume

A larger 2.5hr IVIM local-qCBF hypoperfusion lesion predicted a larger final 4 hr infarct volume (Fig.3). IVIM performed similarly to DSC local-qCBF hypoperfusion (Fig.3B-C) while both outperformed Tmax hypoperfusion (Fig.3A). Local-qCBF hypoperfusion lesions were smaller than the standard-qCBF hypoperfusion lesions (Table 1), though only DSC local-qCBF was statistically significantly smaller than DSC standard-qCBF lesions (p=0.023). DSC standard-qCBF hypoperfusion lesions showed weaker correlation with final infarct volume than local-qCBF ($slope = 3.24, p = 0.06, R^2 = 0.46$ vs. Fig.3B-C).

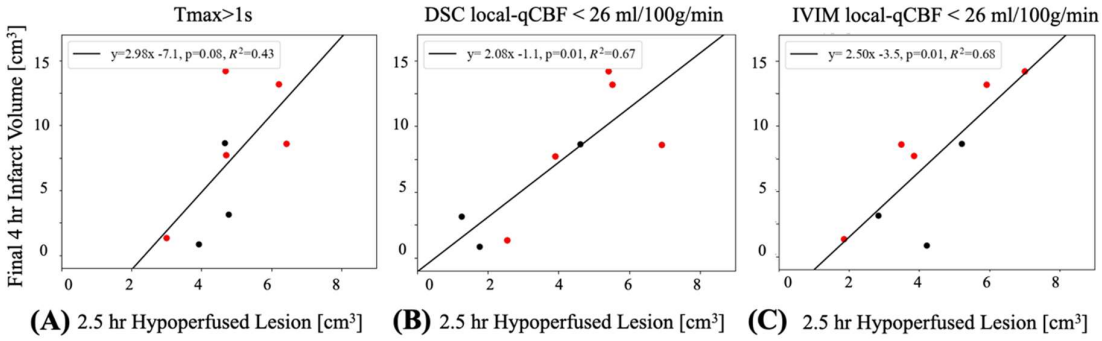

FIG 3. The hypoperfused lesion at 2.5 hours post MCAO was a predictor of final infarct volume for hypoperfusion defined as (A) Tmax>1s, (B) DSC local-qCBF<26 ml/100g/min and (C) IVIM local-qCBF<26 ml/100g/min. Experiments were pooled over treatment and baseline collateralization to expand range of collateral supply. Red represents those that received flow augmentation.

Perfusion-Diffusion Mismatch Ratio and Infarct Growth

The PWI/DWI ratio from Tmax and DSC local-qCBF showed negative correlation with infarct growth (Fig.4A-B). IVIM PWI/DWI ratio returned stronger correlation, potentially due to its ability to capture simultaneous perfusion and diffusion in a single scan and avoiding co-registration or timing mismatch (Fig.4C).

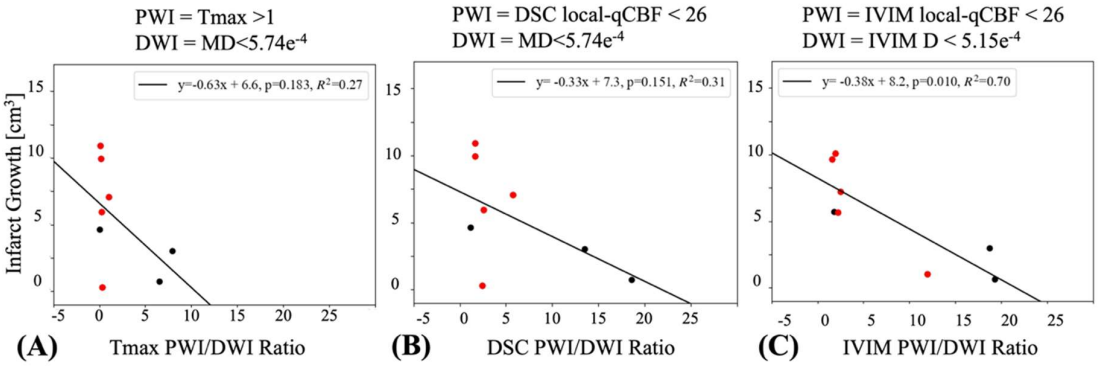

FIG 4. The PWI/DWI ratio of hypoperfused lesion to core infarct at 2.5 hours post MCAO correlated against the infarct growth between the perfusion scan and the final 4-hour infarct. The PWI lesions are defined by thresholding (A) Tmax, (B) DSC local-qCBF, and (C) IVIM local-qCBF. The DWI lesions are defined by (A, B) coregistered mean diffusivity and (C) IVIM D. Experiments were pooled over treatment and baseline collateralization to expand range of collateral supply. Red represents those that received flow augmentation.

Perfusion Time Parameters

Example images of DSC Tmax, DSC MTT, and IVIM WTT are shown for the subjects from Fig.1 as parametric images in Fig.5. Thresholding IVIM WTT at 3s returned the strongest correlation against DSC MTT at 3s ($slope = 0.82, p = 0.04, R^2 = 0.60$). One case was left out of analysis but included in the plot as a yellow outlier (Online Supplemental). This case highlighted the difficulty of fitting IVIM decay to the standard bi-exponential[41], as the curve fit returned low IVIM blood fraction f but normal D^*. This supports the product fD^* being more accurate than individual parameters due to error correlation[42].

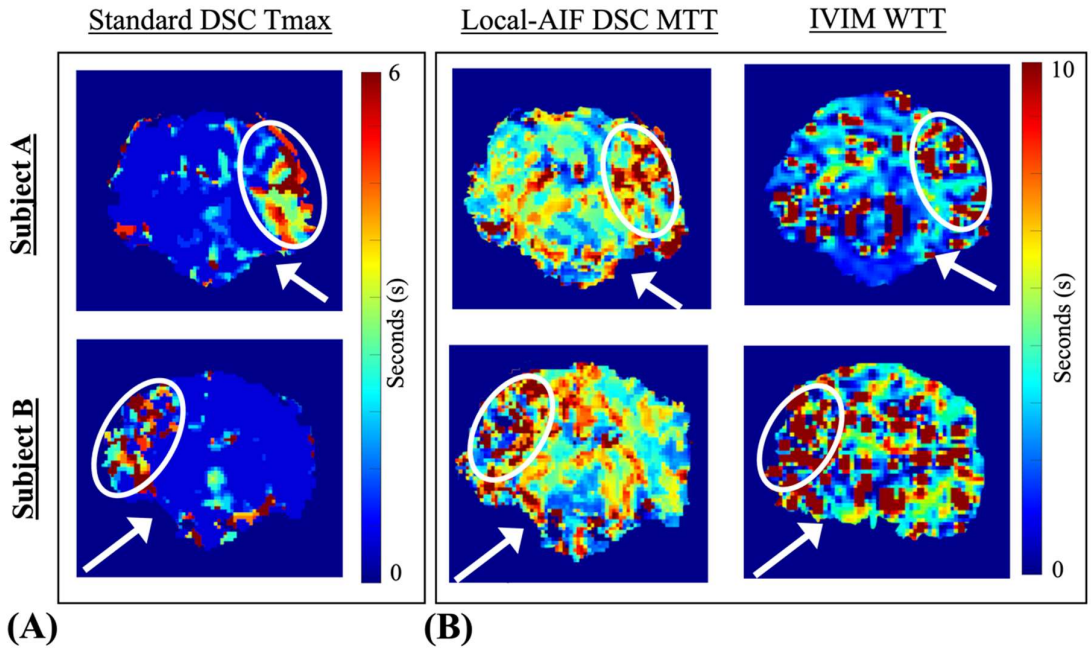

FIG 5. Images of (A) Tmax, and (B) MTT and IVIM WTT for the same Subject A (top row, good collaterals) and Subject B (bottom row, bad collaterals) from Figure 1. Tmax is calculated from standard DSC to capture the delayed arterial bolus. MTT is calculated from Local-AIF DSC to capture local perfusion speed. WTT is the inverse of D* and represents the intravoxel diffusion speed. White arrows denote the position of the MCA coil, white ovals denote the MCA territory. To reduce the fitting sensitivity as the inverse of D*, WTT values over 20s were removed from consideration.

DISCUSSION

This study demonstrated IVIM as a potential method of measuring local-qCBF, including collateral circulation, and perfusion-diffusion mismatch in acute ischemic stroke. DSC and IVIM both independently quantified local-qCBF in ml/100g/min, correlated strongly, and predicted final infarct volume. As DSC local-qCBF has previously been shown to correlate with collateral score[18,19], IVIM local-qCBF correlating strongly with DSC local-qCBF supports IVIM including collateral circulation in acute stroke. Further, these results support combining temporal parameters and volume into blood flow[43] with both DSC local-qCBF and IVIM local-qCBF outperforming Tmax for hypoperfusion and PWI/DWI mismatch. As IVIM is sensitive to local motion of capillary blood, IVIM avoids the complexities of bolus-tracking methods and captures simultaneous quantitative local perfusion and diffusion without contrast agent.

Imaging collateral circulation is valuable to stroke research and therapeutic studies. Even if collateral circulation may arrive delayed and dispersed after having traversed the collateral network, it can still provide vital nutrients and oxygen to prevent infarction. This may explain why good collateral circulation has been shown to influence endovascular treatment outcome[15] as well as time-to-treatment window[44]. As such, PWI/DWI mismatch that includes collateral circulation from local-qCBF may help identify patients with good collaterals who can undergo late thrombectomy safely[5,6,45]. Further, research on novel stroke therapeutics that could boost native collateral circulation to extend the stroke treatment window may also benefit from an ability to image local-qCBF[12,13,26,46,47].

As proposed by Liu et al.[18], collateral circulation can be included in DSC local-qCBF with a local-AIF that corrects delay and dispersion. Further, Federau et al.[19] proposed IVIM "local perfusion fraction" as a measure of collateral blood supply that standard DSC could not capture. The correlation of IVIM local-qCBF to DSC local-qCBF in this current work shows that the two methods of measuring "local perfusion" agree. This supports IVIM including compensatory native and augmented collateral circulation in acute stroke. In addition, IVIM local-qCBF, DSC local-qCBF, and DSC standard-qCBF agreed in the contralateral MCA territory. This supports the difference between local-qCBF and standard-qCBF being due to the collateral circulation in the ipsilateral hemisphere that standard qCBF does not capture.

A subject with higher collateral circulation would be expected to have higher local-qCBF in the ipsilateral MCA territory and smaller final infarct. IVIM local-qCBF demonstrated this trend with higher local-qCBF predicting lower final infarct volume. The use of flow augmentation to boost collateral circulation in this study meant IVIM could not be directly compared to native collateral score. However, as DSC local-qCBF has demonstrated strong correlation with collateral score in previous works, the agreement of IVIM local-qCBF to DSC local-qCBF supports a similar correlation. It should be noted that the flow augmentation in this study was previously observed to increase collateral circulation only in subjects with lower native collaterals[13,26]. This may be why the treatment group (red) in this work did not always return a higher ipsilateral perfusion with smaller final infarct volume than the control group (black) as seen in Fig.2.

The PWI/DWI mismatch ratio showed negative correlation with future infarct growth. The non-infarcted MCA territory may be receiving collateral circulation with reduced blood flow containing vital nutrients and oxygen. However, there is no guarantee that the collateral circulation will be sustained. Interestingly, the PWI/DWI ratio from IVIM measurements outperformed DSC and Tmax in

predicting future infarct growth. As IVIM local-qCBF and DSC local-qCBF themselves showed strong agreement, the improvement of PWI/DWI with IVIM may be due to IVIM imaging simultaneous PWI and DWI, while DSC required a separate DWI MR sequence. Further IVIM PWI and DWI have the same FOV and resolution, while Tmax and DSC did not match the DWI dimensions requiring imperfect co-registration.

The positive bias in the Bland-Altman analysis of IVIM perfusion and DSC perfusion (Fig.2B) may be due to motion other than capillary-level blood such as interstitial fluid and cerebrospinal fluid in subarachnoid space. As IVIM is not contrast or spin-labelled, all motion in a voxel will contribute to signal[36,37]. Since Inversion Recovery to suppress CSF will also suppress blood[23,36], instead an automatic T2 threshold was applied to remove CSF dominated voxels[23,39], and f and D^* were thresholded. However, partial volume contamination could still lead to overestimation of blood signal. Removal with T2prepared CSF suppression[36] could reduce the offset.

Significant correlation of WTT and MTT supports IVIM WTT as an estimation of local transit time, while the offset, reduced correlation at higher thresholds, and outlier highlights limited robustness and the effect of noise in D^*. Mathematically, the inverse of D^*may return falsely high WTT values when $D^*$is fit to a low value. As the D^*parameter alone has shown problems with robustness[48], this work only calculated quantitative qCBF as fD^*averaged across an ROI and for calculation of volumes by thresholding; $D^*$was not used as a quantitative value on a voxel-wise basis nor for visual analysis. Agreeing with literature, f is the more stable terms.

Previous work has found correlation between IVIM and DSC[34,37,40] predominately comparing standard DSC CBV and IVIM f. This avoids the complications of $D^*$and may be more reliable. However, the correlations seen in this study using IVIM local-qCBF and WTT against DSC local-qCBF and MTT show strong correlation, supporting the value of a time component from IVIM and use of a more stable D^*estimation. Further, IVIM local-qCBF and PWI/DWI ratio in acute stroke has not previously been compared to DSC local-qCBF for prediction of final infarct.

As IVIM is non-contrast, it could capture PWI/DWI mismatch throughout infarct progression without issues of multiple contrast injections[31]. The ability to image longitudinal development of potential penumbra, track perfusion-diffusion mismatch over time, and study infarct growth could aid in pre-clinical studies of novel stroke therapeutics. One recent study also supports IVIM in the ischemic penumbra correlating with clinical outcome[49].

This study is not without its limitations. IVIM is still subject to CSF and interstitial fluid contamination, despite use of a T2weighted-threshold. Use of T2preparation IR pulse[36] may be of benefit in future studies. Gd-contrast prevented comparison of IVIM and DSC throughout infarct progression; if Gd is injected multiple times over the development of infarct progression, some contrast will remain and confound quantification of blood flow. An analysis of IVIM local-qCBF and PWI/DWI mismatch, as the stroke develops over time, would be a worthwhile investigation. Difficulties related to fitting IVIM data and noise prevented voxel-wise comparison to DSC MRI; images were analyzed region-by-region, rather than voxel-by-voxel. Further, this work does not study the influence of b-value selection, flow compensation, or cardiac pulsatility. The complexities of the model and physiologic monitoring prevented perfect temporal agreement of DTI, DSC, and IVIM data. Voxel-size and FOV difference prevented perfect co-registration. While heartrate and blood pressure were monitored, fluctuations were inevitable. The conservative number of subjects used in this study limits statistical interpretation and significance. Translation of conclusions derived from animal-based models is a potential limitation, but animal models reduce error in evaluating methods for qCBF calculation with known occlusion time infarct development which is not possible in humans. While a method of imaging PWI/DWI with collateral circulation throughout infarct development has use in pre-clinical research and stroke therapeutics, use of MRI in stroke triage in the US is limited.

CONCLUSIONS

IVIM local-qCBF correlated strongly with DSC local-qCBF, hypoperfusion lesion from DSC local-qCBF and IVIM local-qCBF predicted final infarct volume, and IVIM simultaneous PWI/DWI ratio for ischemic penumbra predicted infarct growth. This supports (1) IVIM as a non-contrast method of local-qCBF that includes collateral circulation, (2) improved agreement of IVIM and DSC with a local-AIF, and (3) IVIM as a viable candidate for longitudinal measurement of simultaneous perfusion and diffusion in pre-clinical stroke research.

ACKNOWLEDGMENTS

The authors would like to acknowledge the support of the US National Institutes of Health R01-NS093908 (Carroll/Christoforidis) and The National Science Foundation DGE-1746045 (Liu).

REFERENCES

1. Rehani B, Ammanuel SG, Zhang Y, et al. A New Era of Extended Time Window Acute Stroke Interventions Guided by Imaging. *The Neurohospitalist*. 2019;10(1):29-37.
2. Fransen PSS, Beumer D, Berkhemer OA, et al. MR CLEAN, a multicenter randomized clinical trial of endovascular treatment for acute ischemic stroke in the Netherlands: study protocol for a randomized controlled trial. *Trials*. 2014;15(1).
3. Goyal M, Jadhav AP, Bonafe A, et al. Analysis of Workflow and Time to Treatment and the Effects on Outcome in Endovascular Treatment of Acute Ischemic Stroke: Results from the SWIFT PRIME Randomized Controlled Trial. *Radiology*. 2016;279(3):888-897.
4. Nogueira RG, Jadhav AP, Haussen DC, et al. Thrombectomy 6 to 24 Hours after Stroke with a Mismatch between Deficit and Infarct. *New England Journal of Medicine*. 2018;378(1):11-21.

5. Olivot J-M, Mlynash M, Thijs VN, et al. Relationships Between Cerebral Perfusion and Reversibility of Acute Diffusion Lesions in DEFUSE. *Stroke*. 2009;40(5):1692-1697.

6. Albers GW, Marks MP, Kemp S, et al. Thrombectomy for Stroke at 6 to 16 Hours with Selection by Perfusion Imaging. *New England Journal of Medicine*. 2018;378(8):708-718.

7. Lansberg MG, Cereda CW, Mlynash M, et al. Response to endovascular reperfusion is not time-dependent in patients with salvageable tissue. *Neurology*. 2015;85(8):708-714.

8. Heiss W-D, Zaro-Weber O. Extension of therapeutic window in ischemic stroke by selective mismatch imaging. *International Journal of Stroke*. 2019;14(4):351-358.

9. Leigh R, Knutsson L, Zhou J, van Zijl PCM. Imaging the physiological evolution of the ischemic penumbra in acute ischemic stroke. *Journal of Cerebral Blood Flow & Metabolism*. 2017;38(9):1500-1516.

10. Demeestere J, Wouters A, Christensen S, Lemmens R, Lansberg MG. Review of Perfusion Imaging in Acute Ischemic Stroke. *Stroke*. 2020;51(3):1017-1024.

11. Christoforidis GA, Saadat N, Liu M, et al. Effect of early Sanguinate (PEGylated carboxyhemoglobin bovine) infusion on cerebral blood flow to the ischemic core in experimental middle cerebral artery occlusion. *J Neurointerv Surg*. 2022;14(12):1253-1257.

12. Shazeeb MS, King RM, Anagnostakou V, et al. Novel Oxygen Carrier Slows Infarct Growth in Large Vessel Occlusion Dog Model Based on Magnetic Resonance Imaging Analysis. *Stroke*. 2022;53(4):1363-1372.

13. Liu M, Saadat N, Jeong YI, et al. Augmentation of perfusion with simultaneous vasodilator and inotropic agents in experimental acute middle cerebral artery occlusion: a pilot study. *J Neurointerv Surg*. 2022.

14. Lansberg MG, Thijs VN, Hamilton S, et al. Evaluation of the Clinical–Diffusion and Perfusion–Diffusion Mismatch Models in DEFUSE. *Stroke*. 2007;38(6):1826-1830.

15. Ribo M, Flores A, Rubiera M, et al. Extending the Time Window for Endovascular Procedures According to Collateral Pial Circulation. *Stroke*. 2011;42(12):3465-3469.

16. Christoforidis GA, Vakil P, Ansari SA, Dehkordi FH, Carroll TJ. Impact of Pial Collaterals on Infarct Growth Rate in Experimental Acute Ischemic Stroke. *AJNR Am J Neuroradiol*. 2017;38(2):270-275.

17. Maguida G, Shuaib A. Collateral Circulation in Ischemic Stroke: An Updated Review. *Journal of Stroke*. 2023;25(2):179-198.

18. Liu M, Saadat N, Roth S, et al. Quantification of Collateral Supply with Local-AIF Dynamic Susceptibility Contrast MRI Predicts Infarct Growth. *AJNR Am J Neuroradiol*. 2024;46(1).

19. Federau C, Wintermark M, Christensen S, et al. Collateral blood flow measurement with intravoxel incoherent motion perfusion imaging in hyperacute brain stroke. *Neurology*. 2019;92(21).

20. Jeong YI, Christoforidis GA, Saadat N, et al. Absolute quantitative MR perfusion and comparison against stable-isotope microspheres. *Magn Reson Med*. 2019;0(0):1-11.

21. Mouannes-Srour JJ, Shin W, Ansari SA, et al. Correction for arterial-tissue delay and dispersion in absolute quantitative cerebral perfusion DSC MR imaging. *Magn Reson Med*. 2012;68(2):495-506.

22. Le Bihan D, Breton E, Lallemand D, Aubin ML, Vignaud J, Laval-Jeantet M. Separation of diffusion and perfusion in intravoxel incoherent motion MR imaging. *Radiology*. 1988;168(2):497-505.

23. Liu M, Saadat N, Jeong Y, et al. Quantitative perfusion and water transport time model from multi b-value diffusion magnetic resonance imaging validated against neutron capture microspheres. *Journal of Medical Imaging*. 2023;10(06).

24. Christoforidis GA, Rink C, Kontzialis MS, et al. An endovascular canine middle cerebral artery occlusion model for the study of leptomeningeal collateral recruitment. *Investigative radiology*. 2011;46(1):34-40.

25. Christoforidis GA, Mohammad Y, Kehagias D, Avutu B, Slivka AP. Angiographic assessment of pial collaterals as a prognostic indicator following intra-arterial thrombolysis for acute ischemic stroke. *AJNR Am J Neuroradiol*. 2005;26(7):1789-1797.

26. Saadat N, Christoforidis GA, Jeong YI, et al. Influence of simultaneous pressor and vasodilatory agents on the evolution of infarct growth in experimental acute middle cerebral artery occlusion. *J Neurointerv Surg*. 2020.

27. Sakaie KE, Shin W, Curtin KR, McCarthy RM, Cashen TA, Carroll TJ. Method for improving the accuracy of quantitative cerebral perfusion imaging. *J Magn Reson Imaging*. 2005;21(5):512-519.

28. Vakil P, Lee JJ, Mouannes-Srour JJ, Derdeyn CP, Carroll TJ. Cerebrovascular occlusive disease: quantitative cerebral blood flow using dynamic susceptibility contrast mr imaging correlates with quantitative H2[15O] PET. *Radiology*. 2013;266(3):879-886.

29. Carroll TJ, Horowitz S, Shin W, et al. Quantification of cerebral perfusion using the "bookend technique": an evaluation in CNS tumors. *Magn Reson Imaging*. 2008;26(10):1352-1359.

30. Carroll TJ, Rowley HA, Haughton VM. Automatic calculation of the arterial input function for cerebral perfusion imaging with MR imaging. *Radiology*. 2003;227(2):593-600.

31. Shin W, Cashen TA, Horowitz SW, Sawlani R, Carroll TJ. Quantitative CBV measurement from static T1 changes in tissue and correction for intravascular water exchange. *Magn Reson Med*. 2006;56(1):138-145.

32. Shin W, Horowitz S, Ragin A, Chen Y, Walker M, Carroll TJ. Quantitative cerebral perfusion using dynamic susceptibility contrast MRI: evaluation of reproducibility and age- and gender-dependence with fully automatic

image postprocessing algorithm. *Magn Reson Med*. 2007;58(6):1232-1241.

33. Shah MK, Shin W, Parikh VS, et al. Quantitative cerebral MR perfusion imaging: preliminary results in stroke. *J Magn Reson Imaging*. 2010;32(4):796-802.
34. Wirestam R, Borg M, Brockstedt S, Lindgren A, Holtas S, Stahlberg F. Perfusion-related parameters in intravoxel incoherent motion MR imaging compared with CBV and CBF measured by dynamic susceptibility-contrast MR technique. *Acta Radiol*. 2001;42(2):123-128.
35. Federau C, Maeder P, O'Brien K, Browaeys P, Meuli R, Hagmann P. Quantitative measurement of brain perfusion with intravoxel incoherent motion MR imaging. *Radiology*. 2012;265(3):874-881.
36. Federau C, O'Brien K. Increased brain perfusion contrast with T2-prepared intravoxel incoherent motion (T2prep IVIM) MRI. *NMR in Biomedicine*. 2014;28(1):9-16.
37. Federau C, Sumer S, Becce F, et al. Intravoxel incoherent motion perfusion imaging in acute stroke: initial clinical experience. *Neuroradiology*. 2014;56(8):629-635.
38. Federau C, O'Brien K, Meuli R, Hagmann P, Maeder P. Measuring brain perfusion with intravoxel incoherent motion (IVIM): initial clinical experience. *J Magn Reson Imaging*. 2014;39(3):624-632.
39. Liu M, Warioba C, Bertini J, et al. Validation and Machine Learning of a New Method for Quantifying CBF with IVIM. American Society of NeuroRadiology Annual Meeting; 2023.
40. Zhu G, Federau C, Wintermark M, et al. Comparison of MRI IVIM and MR perfusion imaging in acute ischemic stroke due to large vessel occlusion. *Int J Stroke*. 2020;15(3):332-342.
41. Shazeeb MS, Sotak CH. Limitations in biexponential fitting of NMR inversion-recovery curves. *Journal of Magnetic Resonance*. 2017;276:14-21.
42. Federau C, O'Brien K, Birbaumer A, Meuli R, Hagmann P, Maeder P. Functional Mapping of the Human Visual Cortex with Intravoxel Incoherent Motion MRI. *Plos One*. 2015;10(2).
43. Nael K, Doshi A, De Leacy R, et al. MR Perfusion to Determine the Status of Collaterals in Patients with Acute Ischemic Stroke: A Look Beyond Time Maps. *American Journal of Neuroradiology*. 2018;39(2):219-225.
44. Hwang YH, Kang DH, Kim YW, Kim YS, Park SP, Liebeskind DS. Impact of Time-to-Reperfusion on Outcome in Patients with Poor Collaterals. *American Journal of Neuroradiology*. 2015;36(3):495-500.
45. Kim SJ, Seok JM, Bang OY, et al. MR Mismatch Profiles in Patients with Intracranial Atherosclerotic Stroke: A Comprehensive approach Comparing Stroke Subtypes. *Journal of Cerebral Blood Flow & Metabolism*. 2009;29(6):1138-1145.
46. Warioba C, Liu M, Penano S, Foxley S, Christoforidis G, Carroll T. Efficacy Assessment of Cerebral Perfusion Augmentation Through Functional Connectivity in an Acute Canine Stroke Model. *American Journal of Neuroradiology*. 2024.
47. King RM, Anagnostakou V, Shazeeb MS, et al. Selective brain cooling with a novel catheter reduces infarct growth after recanalization in a canine large vessel occlusion model. *Interventional Neuroradiology*. 2024.
48. Wu WC, Chen YF, Tseng HM, Yang SC, My PC. Caveat of measuring perfusion indexes using intravoxel incoherent motion magnetic resonance imaging in the human brain. *Eur Radiol*. 2015;25(8):2485-2492.
49. Zimmermann J, Reolon B, Michels L, et al. Intravoxel incoherent motion imaging in stroke infarct core and penumbra is related to long-term clinical outcome. *Scientific Reports*. 2024;14(1).
50. Thomsen BB, Gredal H, Wirenfeldt M, et al. Spontaneous ischaemic stroke lesions in a dog brain: neuropathological characterisation and comparison to human ischaemic stroke. *Acta Vet Scand*. 2017;59(1):7.
51. McHedlishvili G, Kuridze N. The modular organization of the pial arterial system in phylogeny. *J Cereb Blood Flow Metab*. 1984;4(3):391-396.
52. Wu O, Østergaard L, Koroshetz WJ, et al. Effects of tracer arrival time on flow estimates in MR perfusion-weighted imaging. *Magnetic Resonance in Medicine*. 2003;50(4):856-864.
53. Suo S, Cao M, Zhu W, et al. Stroke assessment with intravoxel incoherent motion diffusion-weighted MRI. *NMR in Biomedicine*. 2016;29(3):320-328.
54. Gao QQ, Lu SS, Xu XQ, et al. Quantitative assessment of hyperacute cerebral infarction with intravoxel incoherent motion MR imaging: Initial experience in a canine stroke model. *J Magn Reson Imaging*. 2016;46(2):550-556.
55. Le Bihan D, Breton E, Lallemand D, Grenier P, Cabanis E, Laval-Jeantet M. MR imaging of intravoxel incoherent motions: application to diffusion and perfusion in neurologic disorders. *Radiology*. 1986;161(2):401-407.

SUPPLEMENTAL FILES

APPENDICES

A1. Stroke Model

A2. DSC Global-AIF T1-Bookend Mathematical Theory

A3. DSC Local-AIF Mathematical Theory

A4. Intravoxel Incoherent Motion with Water Transport Time

A5. IVIM Water Transport Time Correlation with DSC Mean Transit Time

A1. Stroke Model

All experiments were conducted using a preclinical canine model of ischemic stroke[24]. The two-day experimental protocol was approved by the University of Chicago Institutional Animal Care and Use Committee and reported in compliance with ARRIVE guidelines. The model was designed to study novel therapeutic techniques for extension of treatment window time in middle cerebral artery occlusion. 83% of the parent study experiments were 'successful' and performed to completion.

The canine model has several advantages as a model for assessment of infarct progression using perfusion and diffusion imaging studies. The neurovascular structure of canines also allows a range of endovascular devices and interventional radiology techniques allowing minimal invasion with real-time visualization of occlusion, preventing imaging artifacts and traumatic cerebrovascular reaction from open surgical occlusion and is a relatively inexpensive alternative to nonhuman primate models of acute ischemia. Canines have a gyrencephalic neocortex with similar ratio of white to grey matter as well as comparable pial arteriolar network organization critical in modeling collateral arterial blood supply and predicting infarct evolution[50,51].

Animals underwent permanent endovascular middle cerebral artery occlusion (MCAO) via embolic occlusion coils at the M1 segment with R/L randomized throughout the experiments. Vertebral and bilateral internal carotid arteriograms confirmed MCAO without involvement of other vessels and assessed pial collateral recruitment. Subjects underwent arteriography and all CBF assessment under general anesthesia. Isoflurane (1% End-Tidal, 0.75 minimum alveolar concentration for canines), propofol infusion (6 mg/kg IV followed by continuous 0.1-0.2 mg/min), and intravenous rocuronium (0.4-0.6 mg/kg every 10-30 minutes) were used to maintain anesthesia with minimal influence on cerebral perfusion. Physiology was monitored via invasive blood pressure, End-Tidal CO_2, O_2 saturation, rectal temperature, heart rate, cardiac rhythm, arterial blood gases, glucose, electrolytes, and hematocrit. Animals were euthanized either the same evening or the following day. Those with unanticipated events such as abnormal baseline MRI, intraprocedural intracranial vessel perforation, or excessive deviation in physiologic parameters during MCAO (presumably from an unanticipated procedural related event) were excluded from this study.

Collateral supply was quantified 30 minutes post-MCAO by assessing X-ray arteriographic images (OEC9800; General Electric Healthcare, Chicago, IL) with a pial collateral score (PCS). PCS is an ordinal score from 1-11, developed for this preclinical model from a score of 1-5 for humans. Scoring was based on the delay and extent of retrograde filling of arterial branches distal to the occluded artery, with 1 being minimal/no collateralization and 11 being retrograde reconstitution of the collateral network up to the occlusion. Subjects with PCS $\leq$8 were considered "poor" and PCS $\geq$ 9 considered "good" collateral supply[13,26]. Poor collaterals demonstrated fast infarct growth while and good collaterals were slow developers.

This current study analyzed only successful controls and flow augmentations subjects of the parent study with completed DSC, IVIM, and DTI sequences. Throughout experiments physiologic parameters were maintained within normal range, excluding blood pressure for experiments involving flow augmentation. Previous work using this model has been published[13,26] but comparison between IVIM and DSC measures of local-qCBF and the expanded collateral circulation with flow augmentation has not been previously examined.

A2. DSC Global-AIF T1-Bookend Mathematical Theory

When contrast is injected via IV, it travels through the heart and lungs and finally to the circle of Willis before perfusing the brain. In dynamic susceptibility contrast MRI, the shape of contrast bolus upon entering the brain represents the global-AIF. When this global-AIF signal is fit to appropriate mathematical models, parameters of interest such a cerebral blood flow, cerebral blood volume, and mean transit time are extracted[30]. The volume of blood in a voxel is proportional to the area under the tissue concentration curve during the first pass of contrast divided by the area under the pure blood curve.

$$\mathrm{rCBV} \propto \frac{\int [\mathrm{Gd}](t)\mathrm{dt}}{\int \text{global-AIF}(t)\mathrm{dt}} \tag{1}$$

To calculate blood flow, the tissue capillary bed can be modeled as a linear system and the AIF can be modeled as a sum of time-shifted and scaled Dirac delta function inputs. The fraction of injected Gadolinium contrast (Gd) in the tissue at time t after the delta input is the residue function, $R(t)$. As the AIF is not instantaneous, it is instead dispersed in time as a narrow curve. This curve can be represented as a set of dirac delta functions at different time delays, i.e. a convolution of the AIF with the residue function.

$$[\mathrm{Gd}](t) = \mathrm{CBF} \times \text{global-AIF}(t) \otimes R(t) \tag{2}$$

Once the global-AIF is chosen there are two unknowns, meaning the residue function scaled by CBF is determined by deconvolution via single value decomposition. Mean transit time (MTT), i.e. the average time a particle traveled through the tissue bed, can then be calculated from the residual.

$$\mathrm{rCBF} \propto \max\big(\mathrm{CBF} \times R(t)\big) \tag{3}$$

$$\mathrm{MTT} = \int R(t) \tag{4}$$

Quantification in ml/100g/min without delay and dispersion corrections is applied via the T1 bookend method[21,28-33]. The DSC scan is bookended by T1 mapping sequences to reduce sensitivity of DSC to AIF selection. Steady-state CBV (qCBV) is calculated using the pre and post T1 maps and used as a calibration factor[27]

$$\mathrm{qCBV} = \frac{\left(\frac{1}{\mathrm{T1_{post}}} - \frac{1}{\mathrm{T1_{pre}}}\right)_{\mathrm{tissue}}}{\left(\frac{1}{\mathrm{T1_{post}}} - \frac{1}{\mathrm{T1_{pre}}}\right)_{\mathrm{blood}}} \tag{5}$$

Water exchange correction factors (WCF) can be determined to account for the residual gadolinium in the blood pool[31] as a function of change in T1 of blood ($\mathrm{R_1}$)

$$\mathrm{WCF} = 0.35\Delta\mathrm{R_1^2} + 0.11\Delta\mathrm{R_1} + 0.06 \tag{6}$$

Combining these returns quantitative cerebral blood flow from conventional DSC.

$$\mathrm{qCBF_{global\text{-}AIF}} = \frac{1}{\rho}\left(\frac{1-\mathrm{Hct_{LV}}}{1-\mathrm{Hct_{SV}}}\right)\left(\frac{\mathrm{qCBV_{SS,WM}}}{\mathrm{rCBV_{DSC,WM}}}\right) \times \mathrm{rCBF_{global\text{-}AIF}} \times \mathrm{WCF} \tag{7}$$

Here $\mathrm{rCBF_{global\text{-}AIF}}$ is the relative CBF calculated from standard deconvolution of the voxel contrast curve deconvolved from the global-AIF. $\mathrm{rCBV_{DSC,WM}}$ is the average relative white matter CBV from the DSC images. $\mathrm{qCBV_{SS,WM}}$ is the average white matter steady-state CBV quantified using the T1 maps. WCF as the water exchange correction factor. ρ is the average density of brain tissue (1.04 g/ml), and $\mathrm{Hct_{LV}}$ and $\mathrm{HCT_{SV}}$ are the hematocrit levels in large (0.45) and small vessels (0.25), respectively. With this we now have quantitative values for all terms in the central volume principal:

$$\mathrm{qCBF\ (ml/100g/min)} = \frac{\mathrm{qCBV\ (ml/100g)}}{\mathrm{MTT\ (min)}} \tag{8}$$

A3. DSC Local-AIF Mathematical Theory

When there is an occlusion of a major artery, blood will have to travel around the occlusion to reach the infarcted hemisphere (Fig.A3). The delay and the dispersion as blood travels through the collateral network can be corrected for with a local-AIF to include collateral supply[52]. With a selection of the global-AIF based on automatic early arrival time and narrow bolus, and selection of venous outflow (VOF) in the sagittal sinus, the strength of delay and dispersion based on arrival time can be calculated as α and β as a function of the time delay $\mathrm{t_D}$ between global-AIF and VOF.

$$\mathrm{VOF}(\mathrm{t}+\mathrm{t_D}) = \frac{\alpha}{(\mathrm{t_D}+1)}\mathrm{e}^{-\frac{\beta \mathrm{t}}{\mathrm{t_D}}} \otimes \mathrm{global\text{-}AIF}(\mathrm{t}) \tag{9}$$

Delay is corrected for as the delay of bolus arrival time to local voxels compared to the global-AIF. Dispersion is corrected for by comparing the bolus shape of the AIF to that of venous outflow at the sagittal sinus. The local-AIF for every voxel with a voxel-specific delay of Δt can be found by deconvolving the global-AIF and the residue function of the VOF using the fit parameters α and β from Eq. 9.

$$\mathrm{local\text{-}AIF}(\mathrm{t}) = \mathrm{global\text{-}AIF}(\mathrm{t}-\Delta\mathrm{t}) \otimes \frac{\alpha}{(\Delta\mathrm{t}+1)}\mathrm{e}^{-\frac{\beta \mathrm{t}}{\Delta \mathrm{t}}} \tag{10}$$

This local-AIF now corrects for delayed arrival time (Δt) and bolus dispersion ($\otimes\ \mathrm{e}^{-\frac{\beta \mathrm{t}}{\Delta \mathrm{t}}}$). Further, the correction term approaches unity at Δt approaches 0, recovering the global result in the absence of delayed and dispersed collateral supply. Replacement of the global-AIF in Eq. 2 and Eq. 7 with the local-AIF that has delay and dispersion correction will return local-AIF perfusion that includes collateral supply and retrograde flow distal to an occlusion.

$$[\mathrm{Gd}](\mathrm{t}) = \mathrm{rCBF_{local\text{-}AIF}} \times \mathrm{global\text{-}AIF}(\mathrm{t}) \otimes \frac{\alpha}{(\Delta\mathrm{t}+1)}\mathrm{e}^{-\frac{\beta \mathrm{t}}{\Delta \mathrm{t}}} \otimes \mathrm{R}(\mathrm{t}) \tag{11}$$

$$\mathrm{qCBF_{local\text{-}AIF}} = \frac{1}{\rho}\left(\frac{1-\mathrm{Hct_{LV}}}{1-\mathrm{Hct_{SV}}}\right)\left(\frac{\mathrm{qCBV_{SS,WM}}}{\mathrm{rCBV_{DSC,WM}}}\right) \times \mathrm{rCBF_{local\text{-}AIF}} \times \mathrm{WCF} \tag{12}$$

Quantitative perfusion calculated with this method of local-AIF DSC has been shown to correlate strongly with pial collateral supply from angiography and infarct growth. Mean transit time can then be calculated from the residual with the local-AIF qCBF in Eq. 12 replacing 'CBF' in Eq.3-4 in Appendix 2.

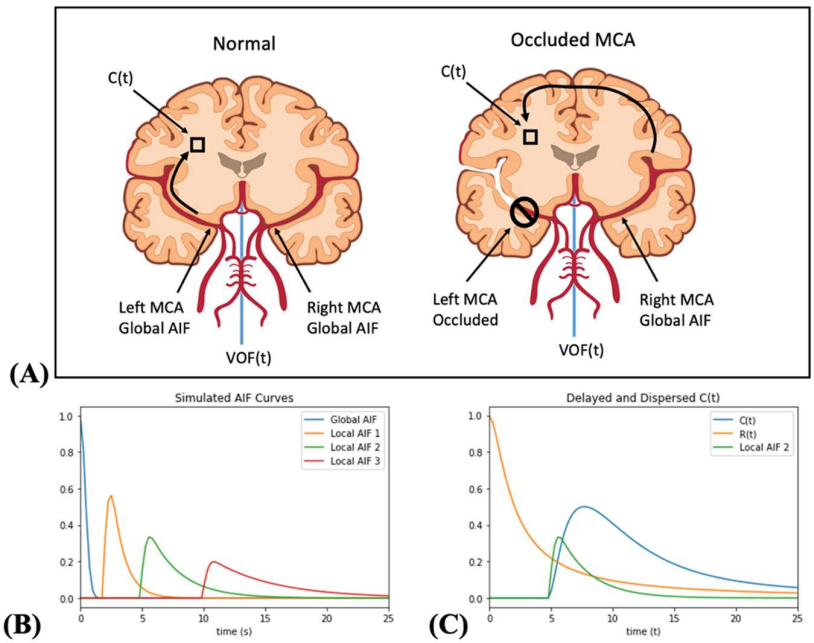

FIG A3. Demonstration of delay and dispersion effects from a global-AIF. A) comparison of blood pathway through the brain from the MCA for a normal (left) and an occluded (right) MCA. B) Examples of simulated local-AIF curves with increasing delay and increasing dispersion. These would be local-AIFs for voxels at increasing distances from the normal hemisphere in A). C) The effect of a delayed and dispersed local-AIF on a contrast curve. If one assumed the global AIF and deconvolves the contrast curve C(t), the Residue function R(t) would be artificially delayed and dispersed due to the longer path. Correction of the delay of contrast arrival will allow inclusion of compensatory perfusion that reaches the occluded hemisphere through the collateral network, rather than through the MCAs. Figure adapted from Liu, M. M. (2023) *Use, Optimization, and Expansion of Quantitative Magnetic Resonance Perfusion Imaging in Cerebrovascular Disease*. [Doctoral Dissertation, University of Chicago]. ProQuest Dissertations Publishing. DOI: doi.org/10.6082/uchicago.7506

A4. Intravoxel Incoherent Motion with Water Transport Time

Intravoxel incoherent motion (IVIM) is a non-contrast MRI is derived from multi b-value diffusion weighted imaging (DWI) and sensitive to intravoxel motion of water in the brain. Unlike DSC which measures hypoperfusion based on a smaller and delayed bolus imaged in a voxel, hypoperfusion with IVIM is measured from *intravoxel* motion, so captures local flow without a need to correct for delayed or dispersed bolus from a major artery. As such, IVIM does not suffer from inaccuracies from AIF selection and can reflect local capillary perfusion within the ischemic penumbra in acute stroke[19,37,53,54]. In IVIM, lower b-values are sensitive to fast diffusion such as perfusing blood, whereas higher b-values probe much slower interstitial water[22,55]. This means that the standard mono-exponential for standard DWI apparent diffusion coefficient (ADC) is expanded into a bi-exponential.

$$\frac{S(b)}{S(0)} = fe^{-bD^*} + (1-f)e^{-bD} \tag{13}$$

In the standard two-compartment model, the first term measures the fraction of signal in a voxel that is blood (f), and its pseudo-diffusion coefficient D^*. The second term represents the remaining signal due to interstitial tissue diffusion $(1-f)$ and the tissue diffusion coefficient (D). Using the multi-compartment Gaussian water transport model returns "Water Transport Time" (analogous to MTT) from the IVIM signal and quantified cerebral blood flow in ml/100g/min[23]. WTT can be solved for by integrating over a 3D sphere and solving for time t at which 50% of the initial molecules have diffused out of the unit sphere.

$$\frac{4\pi}{\left(\sqrt{4\pi D^* t}\right)^3}\int_{0mm}^{.5mm} e^{-\frac{r^2}{4D^* t}} r^2 dr = 0.50 \tag{14}$$

$$WTT = \frac{(.32mm)^2}{2D}\ [s] \tag{15}$$

With assumed values of $\rho = 1.04 g/mL$ and water content fraction $f_w = .79$, this can be plugged into the central volume equation to return perfusion in ml/100g/min as

$$qCBF_{WTT} = \frac{CBV}{WTT} = \frac{f \times f_w}{\rho}\frac{2D^*}{(.32)^2} = fD^* \times \frac{2f_w}{\rho(.32)^2} \approx fD^* \times 93000 \tag{16}$$

As IVIM is based on a multi-b-value acquisition, it also includes high b-values nominally used identification of the infarcted core.

Therefore, by acquiring multiple b-values, a DWI acquisition can estimate simultaneous ADC *and* quantitative tissue perfusion[22] independent of capillary geometry assumptions. Intravoxel motion rather than AIF deconvolution avoids falsely underestimated perfusion due to delayed and dispersed contrast-agent or spin-labelling and therefore should also include compensatory collateral supply like local-AIF DSC.

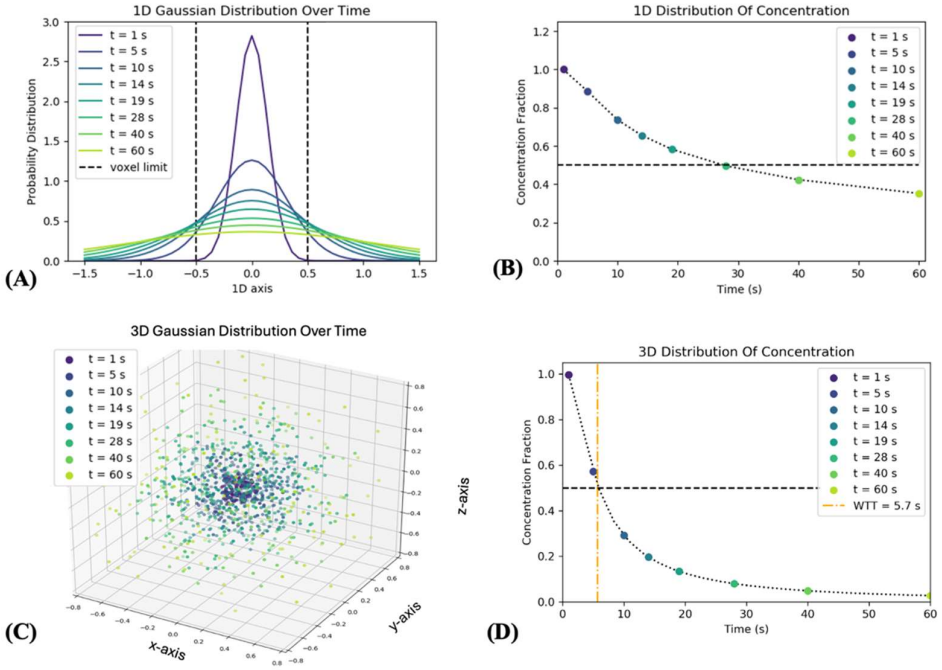

FIG A4. An example of diffusion from 1D and 3D gaussian random walk colorcoded as distributions over time. (A) Demonstrates the change in the 1D probability density function as a function of time, assuming an instantaneous random walk from the center of the voxel, where a voxel is a range along a single line. (B) Demonstrates the change in the concentration in the 1D voxel as a function of time, as expected as particles diffuse, the concentration drops. (C) Demonstrates the change in the 3D density as a function of time, where the voxel would be within the limits of -0.5mm and 0.5mm on all three axes to represent the 1mm unit sphere. (D) Demonstrates the change in that 3D concentration as a function of time from isotropic diffusion. This drop in concentration as the original molecules diffuse out of the sphere is what causes the signal decay in MRI DWI. Figure adapted from Liu, M. M. (2023) *Use, Optimization, and Expansion of Quantitative Magnetic Resonance Perfusion Imaging in Cerebrovascular Disease*. [Doctoral Dissertation, University of Chicago]. ProQuest Dissertations Publishing. DOI: doi.org/10.6082/uchicago.7506

A5. IVIM Water Transport Time Correlation with Local-AIF DSC Mean Transit Time

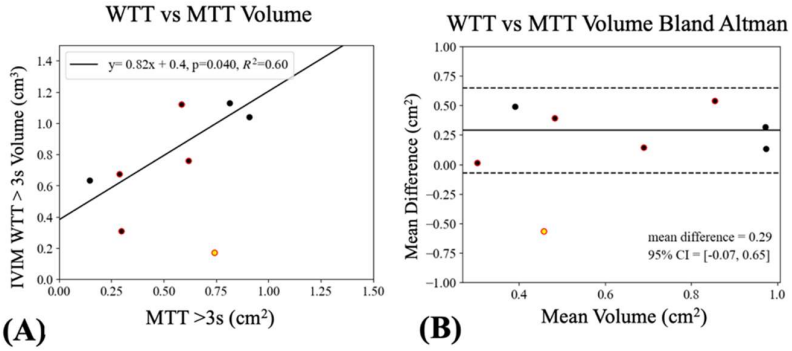

FIG A5. Correlation of (A) Local-AIF DSC MTT>3s volume against IVIM WTT>3s volume. (B) Bland-Altman between MTT and WTT. MTT and WTT represent the mean transit time within a voxel. Thresholded at 3s represents tissue that is perfusing more slowly. Colored yellow is one outlier where the IVIM map had *f* close to zero but normal *D** values that did not indicate slower flow meaning WTT was not heightened. The segmented fit returned low IVIM blood fraction *f* but normal *D**, demonstrating the IVIM parameter product (*fD**) being more accurate than individual parameters, also observed in other work[42].

MRI Protocols from Philips Scanner Export

Contents

SHORT EPI-LL PRE

Patient weight [kg] = 21;
SmartSelect = "yes";
Coil 1 (exclude) = "None";
Uniformity = "CLEAR";
FOV AP (mm) = 160;
RL (mm) = 160;
FH (mm) = 4;
ACQ voxel size AP (mm) = 2.5;
RL (mm) = 2.52873564;
Slice thickness (mm) = 4;
Recon voxel size AP (mm) = 0.909090936;
RL (mm) = 0.909090936;
Fold-over suppression = "no";
Reconstruction matrix = 176;
SENSE = "yes";
P reduction (RL) = 2;
CS-SENSE = "no";
k-t Acceleration = "no";
Stacks = 1;
type = "parallel";
slices = 1;
slice gap = "user defined";
gap (mm) = 0;
slice orientation = "transverse";
fold-over direction = "RL";
fat shift direction = "L";
Stack Offc. AP (P=+mm) = 9.01803112;
RL (L=+mm) = 3.00601959;
FH (H=+mm) = 19.2384758;
Ang. AP (deg) = 0.00189440465;
RL (deg) = -0;
FH (deg) = -0;
Free rotatable = "no";
Slice scan order = "FH";
Large table movement = "no";
PlanAlign = "yes";
REST slabs = 0;
Interactive positioning = "no";
External control = "no";
Patient position = "head first";
Patient body position = "head first";
Patient orientation = "prone";
Patient body orientation = "prone";
Scan type = "Imaging";
Scan mode = "M2D";
technique = "FFE";
Contrast enhancement = "T1";
Acquisition mode = "cartesian";
Fast Imaging mode = "TFEPI";
shot mode = "multishot";
TFE factor = 3;
startup echoes = "user defined";
(number) = 0;
profile order = "low_high";
EPI factor = 5;
Echoes = 1;
partial echo = "no";
shifted echo = "no";
TE = "user defined";
(ms) = 3.5;
Flip angle (deg) = 7;
TR = "user defined";
(ms) = 8;
Halfscan = "no";
Water-fat shift = "user defined";
(pixels) = 2;
RF Shims = "fixed";
Shim = "auto";
mDIXON = "no";
Fat suppression = "no";
Water suppression = "no";
TFE prepulse = "invert";
slice selection = "no";
shared = "yes";
delay = "user defined";
(ms) = 14.3999996;
PSIR = "no";
MTC = "no";
T2prep = "no";
Research prepulse = "no";
Diffusion mode = "no";
T1 mapping = "no";
Transmit channels = "both";
SAR mode = "high";
B1 mode = "default";
SAR allow first level = "yes";
Patient pregnancy = "no";
Patient WB SAR [W/kg] = 0;
Patient Head SAR [W/kg] = 0;
Patient max. dB/dt [T/s] = 0;
Max slewrate [T/m/s] = 0;
Max. B1+rms [uT] = 0;
PNS mode = "high";
Gradient mode = "default";
SofTone mode = "no";
Cardiac synchronization = "trigger";
device = "Internal";
defined phases = 124;
Cycle duration (ms) = 5000;
Heart rate > 250 bpm = "no";
Slice following = "no";
REST grid = "no";
Respiratory compensation = "no";
Navigator respiratory comp = "no";
Flow compensation = "no";
fMRI echo stabilisation = "no";
Motion smoothing = "no";
NSA = 1;
Angio / Contrast enh. = "no";
Quantitative flow = "no";
Manual start = "no";
Dynamic study = "individual";
dyn scans = 1;
dyn scan times = "manual";
fov time mode = "default";
dummy scans = 0;
fast next scan = "no";
dyn stabilization = "no";
prospect. motion corr. = "no";
Keyhole = "no";
Arterial Spin labeling = "no";
Preparation phases = "auto";
Interactive F0 = "no";
Quick Survey = "default";
B0 field map = "no";
B1 field map = "no";
MIP/MPR = "no";
SWIp = "no";
Images = "M", (3) "no";
Autoview image = "M";
Calculated images = (4) "no";
Reference tissue = "Cardiac muscle";
Recon compression = "No";
Preset window contrast = "soft";
Reconstruction mode = "real time";
reuse memory = "no";
Save raw data = "no";
Hardcopy protocol = "no";
Image filter = "system default";
Uniformity correction = "no";
Geometry correction = "default";
Research Options used = "19";
Total scan duration = "00:10.0";
Rel. SNR = 0.254394829;
Act. TR/TE (ms) = "8.0 / 3.5";
Dyn. scan time = "00:10.0";
Time to k0 = "00:05.0";
ACQ matrix M x P = "64 x 60";
ACQ voxel MPS (mm) = "2.50 / 2.67 / 4.00";
REC voxel MPS (mm) = "0.91 / 0.91 / 4.00";
Scan percentage (%) = 93.75;
TFE shots = 2;
TFE dur. shot / acq (ms) = "24.0 / 24.0";
Min. TI delay = 7.07180023;
Phase interval (ms) = 40.1732063;
Max. heart phases = 207;
Act. WFS (pix) / BW (Hz) = "1.923 / 225.9";
BW in EPI freq. dir. (Hz) = "2103.9";
Min. WFS (pix) / Max. BW (Hz) = "1.875 / 231.7";
Min. TR/TE (ms) = "7.5 / 3.4";
Local torso SAR = "< 2 %";
Whole body SAR / level = "< 0.1 W/kg / normal";
SED = " 0.0 kJ/kg";
Coil Power = "2 %";
Max B1+rms = "0.36 uT";
PNS / level = "70 % / normal";
dB/dt = "45.0 T/s";
Sound Pressure Level (dB) = 25.382513;

SHORT EPI-LL POST

Patient weight [kg] = 21;
SmartSelect = "yes";
Coil 1 (exclude) = "None";
Uniformity = "CLEAR";
FOV AP (mm) = 160;
RL (mm) = 160;
FH (mm) = 4;
ACQ voxel size AP (mm) = 2.5;
RL (mm) = 2.52873564;
Slice thickness (mm) = 4;
Recon voxel size AP (mm) = 0.909090936;
RL (mm) = 0.909090936;
Fold-over suppression = "no";
Reconstruction matrix = 176;
SENSE = "yes";
P reduction (RL) = 2;
CS-SENSE = "no";
k-t Acceleration = "no";
Stacks = 1;
type = "parallel";
slices = 1;
slice gap = "user defined";
gap (mm) = 0;
slice orientation = "transverse";
fold-over direction = "RL";
fat shift direction = "L";
Stack Offc. AP (P=+mm) = 9.01803112;
RL (L=+mm) = 3.00601959;
FH (H=+mm) = 19.2384758;
Ang. AP (deg) = 0.00189440465;
RL (deg) = -0;
FH (deg) = -0;
Free rotatable = "no";
Slice scan order = "FH";
Large table movement = "no";
PlanAlign = "yes";
REST slabs = 0;
Interactive positioning = "no";
External control = "no";
Patient position = "head first";
Patient body position = "head first";
Patient orientation = "prone";
Patient body orientation = "prone";
Scan type = "Imaging";
Scan mode = "M2D";
technique = "FFE";
Contrast enhancement = "T1";
Acquisition mode = "cartesian";
Fast Imaging mode = "TFEPI";
shot mode = "multishot";
TFE factor = 3;
startup echoes = "user defined";
(number) = 0;
profile order = "low_high";
EPI factor = 5;
Echoes = 1;
partial echo = "no";
shifted echo = "no";
TE = "user defined";
(ms) = 3.5;
Flip angle (deg) = 7;
TR = "user defined";
(ms) = 8;
Halfscan = "no";
Water-fat shift = "user defined";
(pixels) = 2;
RF Shims = "fixed";
Shim = "auto";
mDIXON = "no";
Fat suppression = "no";
Water suppression = "no";
TFE prepulse = "invert";
slice selection = "no";
shared = "yes";
delay = "user defined";
(ms) = 14.3999996;
PSIR = "no";
MTC = "no";
T2prep = "no";
Research prepulse = "no";
Diffusion mode = "no";
T1 mapping = "no";
Transmit channels = "both";
SAR mode = "high";
B1 mode = "default";
SAR allow first level = "yes";
Patient pregnancy = "no";
Patient WB SAR [W/kg] = 0;
Patient Head SAR [W/kg] = 0;
Patient max. dB/dt [T/s] = 0;
Max slewrate [T/m/s] = 0;
Max. B1+rms [uT] = 0;
PNS mode = "high";
Gradient mode = "default";
SofTone mode = "no";
Cardiac synchronization = "trigger";
device = "Internal";
defined phases = 124;
Cycle duration (ms) = 5000;
Heart rate > 250 bpm = "no";
Slice following = "no";
REST grid = "no";
Respiratory compensation = "no";
Navigator respiratory comp = "no";
Flow compensation = "no";
fMRI echo stabilisation = "no";
Motion smoothing = "no";
NSA = 1;
Angio / Contrast enh. = "no";
Quantitative flow = "no";
Manual start = "no";
Dynamic study = "individual";
dyn scans = 1;
dyn scan times = "manual";
fov time mode = "default";
dummy scans = 0;
fast next scan = "no";
dyn stabilization = "no";
prospect. motion corr. = "no";
Keyhole = "no";
Arterial Spin labeling = "no";
Preparation phases = "auto";
Interactive F0 = "no";
Quick Survey = "default";
B0 field map = "no";
B1 field map = "no";
MIP/MPR = "no";
SWIp = "no";
Images = "M", (3) "no";
Autoview image = "M";
Calculated images = (4) "no";
Reference tissue = "Cardiac muscle";
Recon compression = "No";
Preset window contrast = "soft";
Reconstruction mode = "real time";
reuse memory = "no";
Save raw data = "no";
Hardcopy protocol = "no";
Image filter = "system default";
Uniformity correction = "no";
Geometry correction = "default";
Research Options used = "19";
Total scan duration = "00:10.0";
Rel. SNR = 0.254394829;
Act. TR/TE (ms) = "8.0 / 3.5";
Dyn. scan time = "00:10.0";
Time to k0 = "00:05.0";
ACQ matrix M x P = "64 x 60";
ACQ voxel MPS (mm) = "2.50 / 2.67 / 4.00";
REC voxel MPS (mm) = "0.91 / 0.91 / 4.00";
Scan percentage (%) = 93.75;
TFE shots = 2;
TFE dur. shot / acq (ms) = "24.0 / 24.0";
Min. TI delay = 7.07180023;
Phase interval (ms) = 40.1732063;
Max. heart phases = 207;
Act. WFS (pix) / BW (Hz) = "1.923 / 225.9";
BW in EPI freq. dir. (Hz) = "2103.9";
Min. WFS (pix) / Max. BW (Hz) = "1.875 / 231.7";
Min. TR/TE (ms) = "7.5 / 3.4";
Local torso SAR = "< 2 %";
Whole body SAR / level = "< 0.1 W/kg / normal";
SED = " 0.0 kJ/kg";
Coil Power = "2 %";
Max B1+rms = "0.36 uT";
PNS / level = "70 % / normal";
dB/dt = "45.0 T/s";
Sound Pressure Level (dB) = 25.382513;

LONG EPI-LL PRE

Patient weight [kg] = 21;
SmartSelect = "yes";
Coil 1 (exclude) = "None";
Uniformity = "CLEAR";
FOV RL (mm) = 160;
AP (mm) = 160;
FH (mm) = 4;
ACQ voxel size RL (mm) = 2.5;
AP (mm) = 2.52873564;
Slice thickness (mm) = 4;
Recon voxel size RL (mm) = 0.909090936;
AP (mm) = 0.909090936;
Fold-over suppression = "no";
Reconstruction matrix = 176;
SENSE = "yes";
P reduction (AP) = 2;
CS-SENSE = "no";
k-t Acceleration = "no";
Stacks = 1;
type = "parallel";
slices = 1;
slice gap = "user defined";
gap (mm) = 0;
slice orientation = "transverse";
fold-over direction = "AP";
fat shift direction = "P";
Stack Offc. AP (P=+mm) = 9.01803112;
RL (L=+mm) = 3.00601959;
FH (H=+mm) = 19.2384758;
Ang. AP (deg) = 0.00189440465;
RL (deg) = -0;
FH (deg) = -0;
Free rotatable = "no";
Slice scan order = "FH";
Large table movement = "no";
PlanAlign = "yes";
REST slabs = 0;
Interactive positioning = "no";
External control = "no";
Patient position = "head first";
Patient body position = "head first";
Patient orientation = "prone";
Patient body orientation = "prone";
Scan type = "Imaging";
Scan mode = "M2D";
technique = "FFE";
Contrast enhancement = "T1";
Acquisition mode = "cartesian";
Fast Imaging mode = "TFEPI";
shot mode = "multishot";
TFE factor = 1;
startup echoes = "user defined";
(number) = 0;
profile order = "low_high";
EPI factor = 5;
Echoes = 1;
partial echo = "no";
shifted echo = "no";
TE = "user defined";
(ms) = 3.5;
Flip angle (deg) = 7;
TR = "user defined";
(ms) = 8;
Halfscan = "no";
Water-fat shift = "user defined";
(pixels) = 2;
RF Shims = "fixed";
Shim = "auto";
mDIXON = "no";
Fat suppression = "no";
Water suppression = "no";
TFE prepulse = "invert";
slice selection = "no";
shared = "yes";
delay = "user defined";
(ms) = 14.3999996;
PSIR = "no";
MTC = "no";
T2prep = "no";
Research prepulse = "no";
Diffusion mode = "no";
T1 mapping = "no";
Transmit channels = "both";
SAR mode = "high";
B1 mode = "default";
SAR allow first level = "yes";
Patient pregnancy = "no";
Patient WB SAR [W/kg] = 0;
Patient Head SAR [W/kg] = 0;
Patient max. dB/dt [T/s] = 0;
Max slewrate [T/m/s] = 0;
Max. B1+rms [uT] = 0;
PNS mode = "moderate";
Gradient mode = "default";
SofTone mode = "no";
Cardiac synchronization = "trigger";
device = "Internal";
defined phases = 256;
Cycle duration (ms) = 5000;
Heart rate > 250 bpm = "no";
Slice following = "no";
REST grid = "no";
Respiratory compensation = "no";
Navigator respiratory comp = "no";
Flow compensation = "no";
fMRI echo stabilisation = "no";
Motion smoothing = "no";
NSA = 1;
Angio / Contrast enh. = "no";
Quantitative flow = "no";
Manual start = "no";
Dynamic study = "individual";
dyn scans = 1;
dyn scan times = "manual";
fov time mode = "default";
dummy scans = 0;
fast next scan = "no";
dyn stabilization = "no";
prospect. motion corr. = "no";
Keyhole = "no";
Arterial Spin labeling = "no";
Preparation phases = "auto";
Interactive F0 = "no";
Quick Survey = "default";
B0 field map = "no";
B1 field map = "no";
MIP/MPR = "no";
SWIp = "no";
Images = "M", (3) "no";
Autoview image = "M";
Calculated images = (4) "no";
Reference tissue = "Cardiac muscle";
Recon compression = "No";
Preset window contrast = "soft";
Reconstruction mode = "real time";
reuse memory = "no";
Save raw data = "no";
Hardcopy protocol = "no";
Image filter = "system default";
Uniformity correction = "no";
Geometry correction = "default";
Research Options used = "19";
Total scan duration = "00:30.0";
Rel. SNR = 0.254394829;
Act. TR/TE (ms) = "8.0 / 3.5";
Dyn. scan time = "00:30.0";
Time to k0 = "00:15.0";
ACQ matrix M x P = "64 x 60";
ACQ voxel MPS (mm) = "2.50 / 2.67 / 4.00";
REC voxel MPS (mm) = "0.91 / 0.91 / 4.00";
Scan percentage (%) = 93.75;
TFE shots = 6;
TFE dur. shot / acq (ms) = "8.0 / 8.0";
Min. TI delay = 7.07180023;
Phase interval (ms) = 8;
Max. heart phases = 256;
Act. WFS (pix) / BW (Hz) = "1.923 / 225.9";
BW in EPI freq. dir. (Hz) = "2103.9";
Min. WFS (pix) / Max. BW (Hz) = "1.875 / 231.7";
Min. TR/TE (ms) = "7.5 / 3.4";
Local torso SAR = "< 2 %";
Whole body SAR / level = "< 0.1 W/kg / normal";
SED = " 0.0 kJ/kg";
Coil Power = "2 %";
Max B1+rms = "0.34 uT";
PNS / level = "59 % / normal";
dB/dt = "45.0 T/s";
Sound Pressure Level (dB) = 27.5770683;

LONG EPI-LL POST

Patient weight [kg] = 21;
SmartSelect = "yes";
Coil 1 (exclude) = "None";
Uniformity = "CLEAR";
FOV RL (mm) = 160;
AP (mm) = 160;
FH (mm) = 4;
ACQ voxel size RL (mm) = 2.5;
AP (mm) = 2.52873564;
Slice thickness (mm) = 4;
Recon voxel size RL (mm) = 0.909090936;
AP (mm) = 0.909090936;
Fold-over suppression = "no";
Reconstruction matrix = 176;
SENSE = "yes";
P reduction (AP) = 2;
CS-SENSE = "no";
k-t Acceleration = "no";
Stacks = 1;
type = "parallel";
slices = 1;
slice gap = "user defined";
gap (mm) = 0;
slice orientation = "transverse";
fold-over direction = "AP";
fat shift direction = "P";
Stack Offc. AP (P=+mm) = 9.01803112;
RL (L=+mm) = 3.00601959;
FH (H=+mm) = 19.2384758;
Ang. AP (deg) = 0.00189440465;
RL (deg) = -0;
FH (deg) = -0;
Free rotatable = "no";
Slice scan order = "FH";
Large table movement = "no";
PlanAlign = "yes";
REST slabs = 0;
Interactive positioning = "no";
External control = "no";
Patient position = "head first";
Patient body position = "head first";
Patient orientation = "prone";
Patient body orientation = "prone";
Scan type = "Imaging";
Scan mode = "M2D";
technique = "FFE";
Contrast enhancement = "T1";
Acquisition mode = "cartesian";
Fast Imaging mode = "TFEPI";
shot mode = "multishot";
TFE factor = 1;
startup echoes = "user defined";
(number) = 0;
profile order = "low_high";
EPI factor = 5;
Echoes = 1;
partial echo = "no";
shifted echo = "no";
TE = "user defined";
(ms) = 3.5;
Flip angle (deg) = 7;
TR = "user defined";
(ms) = 8;
Halfscan = "no";
Water-fat shift = "user defined";
(pixels) = 2;
RF Shims = "fixed";
Shim = "auto";
mDIXON = "no";
Fat suppression = "no";
Water suppression = "no";
TFE prepulse = "invert";
slice selection = "no";
shared = "yes";
delay = "user defined";
(ms) = 14.3999996;
PSIR = "no";
MTC = "no";
T2prep = "no";
Research prepulse = "no";
Diffusion mode = "no";
T1 mapping = "no";
Transmit channels = "both";
SAR mode = "high";
B1 mode = "default";
SAR allow first level = "yes";
Patient pregnancy = "no";
Patient WB SAR [W/kg] = 0;
Patient Head SAR [W/kg] = 0;
Patient max. dB/dt [T/s] = 0;
Max slewrate [T/m/s] = 0;
Max. B1+rms [uT] = 0;
PNS mode = "moderate";
Gradient mode = "default";
SofTone mode = "no";
Cardiac synchronization = "trigger";
device = "Internal";
defined phases = 256;
Cycle duration (ms) = 5000;
Heart rate > 250 bpm = "no";
Slice following = "no";
REST grid = "no";
Respiratory compensation = "no";
Navigator respiratory comp = "no";
Flow compensation = "no";
fMRI echo stabilisation = "no";
Motion smoothing = "no";
NSA = 1;
Angio / Contrast enh. = "no";
Quantitative flow = "no";
Manual start = "no";
Dynamic study = "individual";
dyn scans = 1;
dyn scan times = "manual";
fov time mode = "default";
dummy scans = 0;
fast next scan = "no";
dyn stabilization = "no";
prospect. motion corr. = "no";
Keyhole = "no";
Arterial Spin labeling = "no";
Preparation phases = "auto";
Interactive F0 = "no";
Quick Survey = "default";
B0 field map = "no";
B1 field map = "no";
MIP/MPR = "no";
SWIp = "no";
Images = "M", (3) "no";
Autoview image = "M";
Calculated images = (4) "no";
Reference tissue = "Cardiac muscle";
Recon compression = "No";
Preset window contrast = "soft";
Reconstruction mode = "real time";
reuse memory = "no";
Save raw data = "no";
Hardcopy protocol = "no";
Image filter = "system default";
Uniformity correction = "no";
Geometry correction = "default";
Research Options used = "19";
Total scan duration = "00:30.0";
Rel. SNR = 0.254394829;
Act. TR/TE (ms) = "8.0 / 3.5";
Dyn. scan time = "00:30.0";
Time to k0 = "00:15.0";
ACQ matrix M x P = "64 x 60";
ACQ voxel MPS (mm) = "2.50 / 2.67 / 4.00";
REC voxel MPS (mm) = "0.91 / 0.91 / 4.00";
Scan percentage (%) = 93.75;
TFE shots = 6;
TFE dur. shot / acq (ms) = "8.0 / 8.0";
Min. TI delay = 7.07180023;
Phase interval (ms) = 8;
Max. heart phases = 256;
Act. WFS (pix) / BW (Hz) = "1.923 / 225.9";
BW in EPI freq. dir. (Hz) = "2103.9";
Min. WFS (pix) / Max. BW (Hz) = "1.875 / 231.7";
Min. TR/TE (ms) = "7.5 / 3.4";
Local torso SAR = "< 2 %";
Whole body SAR / level = "< 0.1 W/kg / normal";
SED = " 0.0 kJ/kg";
Coil Power = "2 %";
Max B1+rms = "0.34 uT";
PNS / level = "59 % / normal";
dB/dt = "45.0 T/s";
Sound Pressure Level (dB) = 27.5770683;

FE EPI

Patient weight [kg] = 21;
SmartSelect = "yes";
Coil 1 (exclude) = "None";
Uniformity = "CLEAR";
FOV AP (mm) = 160;
RL (mm) = 160;
FH (mm) = 38;
ACQ voxel size AP (mm) = 2;
RL (mm) = 2.02531648;
Slice thickness (mm) = 6;
Recon voxel size AP (mm) = 0.909090936;
RL (mm) = 0.909090936;
Fold-over suppression = "no";
Reconstruction matrix = 176;
SENSE = "yes";
P reduction (RL) = 2.29999995;
MB SENSE = "no";
CS-SENSE = "no";
k-t Acceleration = "no";
Stacks = 1;
type = "parallel";
slices = 5;
slice gap = "user defined";
gap (mm) = 2;
slice orientation = "transverse";
fold-over direction = "RL";
fat shift direction = "L";
Stack Offc. AP (P=+mm) = 9.01803112;
RL (L=+mm) = 3.00601959;
FH (H=+mm) = 19.2384758;
Ang. AP (deg) = 0.00189440465;
RL (deg) = -0;
FH (deg) = -0;
Free rotatable = "no";
Minimum number of packages = 1;
Slice scan order = "FH";
Large table movement = "no";
PlanAlign = "yes";
REST slabs = 0;
Interactive positioning = "no";
External control = "no";
Patient position = "head first";
Patient body position = "head first";
Patient orientation = "prone";
Patient body orientation = "prone";
Scan type = "Imaging";
Scan mode = "MS";
technique = "FFE";
Contrast enhancement = "no";
Acquisition mode = "cartesian";
Fast Imaging mode = "EPI";
shot mode = "single-shot";
Echoes = 1;
partial echo = "no";
shifted echo = "no";
TE = "user defined";
(ms) = 30;
Flip angle (deg) = 75;
TR = "user defined";
(ms) = 500;
Halfscan = "no";
Water-fat shift = "minimum";
RF Shims = "fixed";
Shim = "auto";
mDIXON = "no";
Fat suppression = "SPIR";
strength = "strong";
frequency offset = "user defined";
offset (Hz) = 135;
Water suppression = "no";
MTC = "no";
Research prepulse = "no";
Diffusion mode = "no";
T1 mapping = "no";
Transmit channels = "both";
SAR mode = "high";
B1 mode = "default";
SAR allow first level = "yes";
Patient pregnancy = "no";
Patient WB SAR [W/kg] = 0;
Patient Head SAR [W/kg] = 0;
Patient max. dB/dt [T/s] = 0;
Max slewrate [T/m/s] = 0;
Max. B1+rms [uT] = 0;
PNS mode = "high";
Gradient mode = "maximum";
SofTone mode = "no";
Cardiac synchronization = "no";
Heart rate > 250 bpm = "no";
Respiratory compensation = "no";
Navigator respiratory comp = "no";
Flow compensation = "no";
Temporal slice spacing = "default";
fMRI echo stabilisation = "no";
NSA = 1;
Angio / Contrast enh. = "no";
Quantitative flow = "no";
Manual start = "yes";
Dynamic study = "individual";
dyn scans = 200;
dyn scan times = "shortest";
fov time mode = "default";
dummy scans = 0;
immediate subtraction = "no";
fast next scan = "no";
synch. ext. device = "no";
dyn stabilization = "no";
prospect. motion corr. = "no";
Keyhole = "no";
Arterial Spin labeling = "no";
Preparation phases = "auto";
Interactive F0 = "no";
Quick Survey = "default";
B0 field map = "no";
B1 field map = "no";
MIP/MPR = "no";
SWIp = "no";
Images = "M", (3) "no";
Autoview image = "M";
Calculated images = (4) "no";
Reference tissue = "Grey matter";
Recon compression = "No";
Preset window contrast = "soft";
Reconstruction mode = "real time";
reuse memory = "no";
Save raw data = "no";
Hardcopy protocol = "no";
Image filter = "system default";
Uniformity correction = "no";
Geometry correction = "default";
Total scan duration = "01:42.0";
Rel. SNR = 1.42417169;
Act. TR/TE (ms) = "500 / 30";
Dyn. scan time = "0.500";
Time to k0 = "0.250";
ACQ matrix M x P = "80 x 80";
ACQ voxel MPS (mm) = "2.00 / 2.00 / 6.00";
REC voxel MPS (mm) = "0.91 / 0.91 / 6.00";
Scan percentage (%) = 100;
Packages = 1;
Min. slice gap (mm) = -0;
EPI factor = 35;
Act. WFS (pix) / BW (Hz) = "10.891 / 39.9";
BW in EPI freq. dir. (Hz) = "1769.8";
Min. WFS (pix) / Max. BW (Hz) = "10.256 / 42.4";
Min. TR/TE (ms) = "274 / 14";
SPIR offset act./default (Hz) = "135 [220]";
Local torso SAR = "< 18 %";
Whole body SAR / level = "< 0.6 W/kg / normal";
SED = "< 0.1 kJ/kg";
Coil Power = "17 %";
Max B1+rms = "0.96 uT";
PNS / level = "92 % / 1st level";
dB/dt = "112.6 T/s";
Sound Pressure Level (dB) = 22.9644241;

IVIM

Patient weight [kg] = 21;
SmartSelect = "yes";
Coil 1 (exclude) = "None";
Uniformity = "CLEAR";
FOV RL (mm) = 160;
AP (mm) = 160;
FH (mm) = 100;
ACQ voxel size RL (mm) = 2;
AP (mm) = 2;
Slice thickness (mm) = 2;
Recon voxel size RL (mm) = 1.66666663;
AP (mm) = 1.66666663;
Fold-over suppression = "no";
Reconstruction matrix = 96;
SENSE = "yes";
P reduction (AP) = 2;
MB SENSE = "no";
CS-SENSE = "no";
k-t Acceleration = "no";
Stacks = 1;
type = "parallel";
slices = 50;
slice gap = "user defined";
gap (mm) = 0;
slice orientation = "transverse";
fold-over direction = "AP";
fat shift direction = "P";
Stack Offc. AP (P=+mm) = 0;
RL (L=+mm) = 4.20842171;
FH (H=+mm) = 30.0601387;
Ang. AP (deg) = 0.00189440465;
RL (deg) = -0;
FH (deg) = -0;
Free rotatable = "no";
Minimum number of packages = 2;
Slice scan order = "default";
Large table movement = "no";
PlanAlign = "yes";
REST slabs = 0;
Interactive positioning = "no";
External control = "no";
Patient position = "head first";
Patient body position = "head first";
Patient orientation = "prone";
Patient body orientation = "prone";
Scan type = "Imaging";
Scan mode = "MS";
technique = "SE";
Modified SE = "no";
Acquisition mode = "cartesian";
Fast Imaging mode = "EPI";
shot mode = "single-shot";
Echoes = 1;
partial echo = "no";
TE = "user defined";
(ms) = 120;
Flip angle (deg) = 90;
TR = "shortest";
Halfscan = "yes";
factor = 0.847458005;
Water-fat shift = "minimum";
RF Shims = "fixed";
Shim = "auto";
mDIXON = "no";
Fat suppression = "SPIR";
strength = "strong";
frequency offset = "user defined";
offset (Hz) = 135;
Grad Rev Fat suppr = "yes";
Water suppression = "no";
BB pulse = "no";
MTC = "no";
APT = "no";
Research prepulse = "no";
Diffusion mode = "DWI";
sequence = "SE";
gradient expert mode = "no";
gradient overplus = "no";
direction = "M", "P", "S";
nr of b-factors = 10;
b-factor order = "ascending";
max b-factor = 1000;
average high b = "no";
T1 mapping = "no";
Transmit channels = "both";
SAR mode = "high";
B1 mode = "default";
SAR allow first level = "yes";
Patient pregnancy = "no";
Patient WB SAR [W/kg] = 0;
Patient Head SAR [W/kg] = 0;
Patient max. dB/dt [T/s] = 0;
Max slewrate [T/m/s] = 0;
Max. B1+rms [uT] = 0;
PNS mode = "moderate";
Gradient mode = "default";
SofTone mode = "no";
Cardiac synchronization = "no";
Heart rate > 250 bpm = "no";
Respiratory compensation = "no";
Navigator respiratory comp = "no";
Flow compensation = "no";
Temporal slice spacing = "default";
NSA = 2;
SMART = "no";
Manual start = "no";
Dynamic study = "no";
Arterial Spin labeling = "no";
Preparation phases = "auto";
Interactive F0 = "no";
Quick Survey = "default";
B0 field map = "no";
B1 field map = "no";
MIP/MPR = "no";
Images = "M", (3) "no";
Autoview image = "M";
Calculated images = (4) "no";
Reference tissue = "White matter";
Recon compression = "No";
Preset window contrast = "soft";
Reconstruction mode = "immediate";
Save raw data = "no";
Hardcopy protocol = "no";
Image filter = "system default";
Uniformity correction = "no";
Geometry correction = "default";
Total scan duration = "07:10.3";
Rel. SNR = 1;
Act. TR (ms) = "3775";
Act. TE (ms) = "120";
ACQ matrix M x P = "80 x 78";
ACQ voxel MPS (mm) = "2.00 / 2.05 / 2.00";
REC voxel MPS (mm) = "1.67 / 1.67 / 2.00";
Scan percentage (%) = 97.5;
Packages = 2;
Min. slice gap (mm) = -0;
EPI factor = 39;
WFS (pix) / BW (Hz) = "13.607 / 31.9";
BW in EPI freq. dir. (Hz) = "1770.8";
SPIR offset act./default (Hz) = "135 [220]";
Local torso SAR = "< 27 %";
Whole body SAR / level = "< 0.9 W/kg / normal";
SED = "< 0.4 kJ/kg";
Coil Power = "25 %";
Max B1+rms = "1.18 uT";
PNS / level = "67 % / normal";
dB/dt = "62.4 T/s";
Sound Pressure Level (dB) = 18.1809082;